LETTER Communicated by Peter Rowat

On the Phase-Space Dynamics of Systems of Spiking Neurons. I: Model and Experiments

Arunava Banerjee
Department of Computer Science, Rutgers, The State University of New Jersey, Piscataway, NJ 08854, U.S.A.

We investigate the phase-space dynamics of a general model of local systems of biological neurons in order to deduce the salient dynamical characteristics of such systems. In this article, we present a detailed exposition of an abstract dynamical system that models systems of biological neurons. The abstract system is based on a limited set of realistic assumptions and thus accommodates a wide range of neuronal models. Simulation results are presented for several instantiations of the abstract system, each modeling a typical neocortical column to a different degree of accuracy. The results demonstrate that the dynamics of the systems are generally consistent with that observed in neurophysiological experiments. They reveal that the qualitative behavior of the class of systems can be classified into three distinct categories: quiescence, intense periodic activity resembling a state of seizure, and sustained chaos over the range of intrinsic activity typically associated with normal operational conditions in the neocortex. We discuss basic ramifications of this result with regard to the computational nature of neocortical neuronal systems.

1 Introduction

Our understanding of the computational nature of systems of interconnected neuron-like elements has grown steadily over the past decades (Hopfield, 1982; Amit, Gutfreund, & Sompolinsky, 1987; Hornik, Stinchcombe, & White, 1989; Siegelmann & Sontag, 1992; Omlin & Giles, 1996, to mention but a few). The extent to which some of these results apply to systems of neurons in the brain, however, remains uncertain, primarily because the models of the neurons, as well as those of the networks used in such studies, do not sufficiently resemble their biological counterparts.

The past decade has also been witness to several theories advanced to explain the observed behavioral properties of large fields of neurons in the brain (Nunez, 1989; Wright, 1990; Freeman, 1991). In general, these models do not adopt the neuron as their basic functional unit; for example, Freeman's model utilizes the KI, KII, and KIII configurations of neurons as its basic units, and Wright's model lumps small cortical areas into single functional units. Moreover, some of these models are founded on presupposed

functional properties of the macroscopic phenomenon under investigation; for example, Wright's and Nunez's models assume that the global wavelike processes revealed in EEG recordings satisfy linear dynamics. These reasons account, in part, for the controversies that surround these theories.

The search for coherent structures in the dynamics of neuronal systems has also seen a surge of activity (Basar, 1990; Krüger, 1991a; Aertsen & Braitenberg, 1992; Bower & Beeman, 1995). Armed with faster and more powerful computers, scientists are replicating salient patterns of activity observed in neuronal systems in phenomena as diverse as motor behavior in animals and oscillatory activity in the cortex. The models of the neurons as well as those of the networks are considerably more realistic in these cases. There is an emphasis on simulation, and it is hoped that analytic insight will be forthcoming from such experimentation.

Our research shares the broad objectives of these diverse endeavors: to unravel the dynamical and computational properties of systems of neurons in the brain. Our goal, in particular, is to answer two crucial questions: (1) Are there coherent spatiotemporal structures in the dynamics of neuronal systems that can denote symbols[1] and (2) If such structures exist, what restrictions do the dynamics of the system at the physical level impose on the dynamics of the system at the corresponding abstracted symbolic level?

Our approach is characterized by our position on two significant methodological issues. First, we take a conservative bottom-up approach to the problem, that is, we adopt the biological neuron as our basic functional unit,[2] and second, given the generalized nature of the questions posed, we believe that answers can be obtained primarily through the analysis of the phase-space dynamics of an abstract dynamical system whose behavior sufficiently matches that of the biological system.

The first part of this article is devoted to the construction of such a dynamical system. In section 2, we identify a general set of characteristics of a biological neuron and formulate a model of a neuron based on them. In section 3, we construct the phase-space for a system of such neurons. The geometric structure immanent in the phase-space is also described in detail. Finally in section 4, we specify the velocity field that overlays the phase-space, thereby completing the construction of the abstract dynamical system.

Section 5 is devoted to a numerical investigation of the dynamics of the system. A typical neocortical column is modeled based on anatomical and

[1] Our usage of the term *symbol* conforms with the limited notion of a symbol as used in computer science—discrete states that mark a computational process regardless of representational content, if any, and not the notion of a symbol in the greater sense of the word—(the physical embodiment of a semantic unit) as used in the cognitive sciences. This work therefore does not take a position on the contentious issue of representationalism.

[2] We believe that by not assuming a lumped unit with presupposed functional characteristics, we not only detract from controversy but also add to the well-foundedness of the theory.

physiological data. Several instantiations, of varying degrees of accuracy, are examined. The results of the simulations demonstrate that the dynamics of the systems are generally consistent with that observed in neurophysiological experiments. They also highlight certain dynamical properties that are robust across the instantiations.

The results reveal that the qualitative behavior of the class of systems can be classified into three distinct categories: (1) when initiated at a low level of intrinsic activity, the system becomes quiescent; (2) when initiated at a high level of intrinsic activity, the system settles into a periodic orbit of intense regular activity resembling a state of seizure; and (3) when initiated over a range of intermediate levels of intrinsic activity (corresponding to normal operational conditions in the neocortex), the system displays sustained chaotic behavior.

In section 6 we discuss basic ramifications of this result with regard to the computational nature of neocortical neuronal systems. The questions posed earlier in this section are partially answered, and a research agenda, pursued in the companion article in this issue, is proposed for a definite resolution of the matter.

2 Model of the Neuron

We have chosen a deterministic (as opposed to a stochastic) model for the biological neuron for the following reasons. First, there is mounting evidence that information about stimulus is contained in the higher-resolution interspike intervals (ISIs) of spike trains and not in the lower-resolution spike frequencies (Strehler & Lestienne, 1986; Krüger, 1991b; Bair, Koch, Newsome, & Britten, 1994; Bair & Koch, 1996). Since the temporal sequence of ISIs is abstracted away in a stochastic model, there is little hope that such a model would shed light on all aspects of information processing in neuronal systems. Second, while random miniature postsynaptic potentials do exist, their mean amplitude is at least an order of magnitude smaller than the mean amplitude of the postsynaptic potential elicited by the arrival of a spike at a synapse. The impact of such noise on the dynamics of the system is best identified by contrasting the dynamics of a noise-free model to that of a model augmented with the appropriate noise. It is therefore logical to begin with the analysis of a deterministic model.

Our model of the biological neuron is based on the following four observations:

1. The biological neuron is a finite precision machine in the sense that the depolarization at the soma that elicits an action potential is of a finite range ($\mathcal{T} \pm \epsilon$) and not a precise value ($\mathcal{T}$).
2. The effect of a synaptic impulse (resulting from the arrival of an afferent (incoming) spike) at the soma has the characteristic form

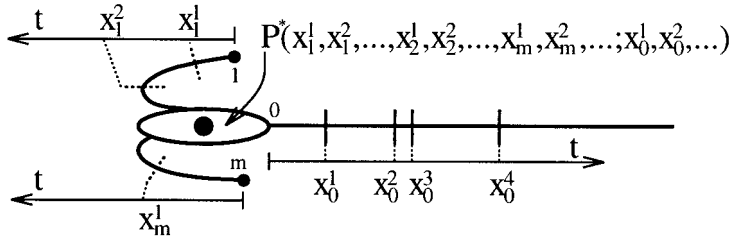

Figure 1: A schematic diagram of a neuron that depicts the soma, axon, and two synapses on as many dendrites. The axes by the synapses and the axon denote time (with respective origins set at present and the direction of the arrows indicating past). Spikes on the axon are depicted as solid lines. Those on the dendrites are depicted as broken lines, for, having been converted into graded potentials, their existence is only abstract (point objects indicating the time of arrival of the spike).

of an abrupt increase or decrease in potential followed by a longer exponential-like decay toward the resting level.

3. The postspike elevation of the threshold that may be modeled as the inhibitory effect of an efferent (outgoing) spike also decays after a while at an exponential rate.
4. The ISIs of any given neuron are bounded from below by its absolute refractory period, r, that is, no two spikes originate closer than r in time.

Based on these, we construct our model of the neuron as follows. (Figure 1 is provided as a visual aid to complement the formal presentation below. The various aspects of the diagram are explained in the caption.)

i. **Spikes**. Spikes are the sole bearers of information. They are identical except for their spatiotemporal location. (Spikes are defined as point objects. Although action potentials are not instantaneous, they can always be assigned occurrence times, which may, for example, be the time at which the membrane potential at the soma reached the threshold $\mathcal{T}$.)

ii. **Membrane potential**. For any given neuron we assume an implicit, C^∞, everywhere bounded function $P^*(\vec{x}_1, \vec{x}_2, \ldots, \vec{x}_m; \vec{x}_0)$ that yields the current membrane potential at the soma. (Subscripts $i = 1, \ldots, m$ represent the afferent synapses, and $\vec{x}_i = \langle x_i^1, x_i^2, \ldots, x_i^j, \ldots \rangle$ is a denumerable sequence of variables that represent, for spikes arriving at synapse i since infinite past, the time lapsed since their arrivals. In other words, each x_i^j for $i = 1, \ldots, m$ reports the time interval between the present and the time of arrival of a distinct spike at synapse

i. Finally, $\vec{x}_0$ is a denumerable sequence of variables that represent, in like manner, the time lapsed since the departure of individual spikes generated at the soma of the neuron.)

P^*: $\mathbb{R}^\infty \rightarrow \mathbb{R}$ accounts for the entire spatiotemporal aspect of the neuron's response to spikes. All information regarding the strength of afferent synapses, their location on the dendrites, and their modulation of one another's effects at the soma is implicitly contained within $P^*(\cdot)$. So is the exact nature of the postspike hyperpolarization that gives rise to both the absolute and the relative refractory periods. Consistency requires that either the domain of $P^*(\cdot)$ be restricted to $0 \leq x_i^1 \leq x_i^2 \leq \cdots$ for all i, or $P^*(\cdot)$ be constrained to be symmetric with respect to $x_i^1, x_i^2, \ldots$ for all i.

iii. **Effectiveness of a Spike**. After the effect of a spike at the soma of a biological neuron has decayed below $\frac{\epsilon}{C(m+1)}$, where ϵ is the range of error of the threshold, $C > 1$ an appropriate constant (defined below), and m the number of afferent synapses on the cell, its effectiveness on the neuron expires. This inference is based on the observations that the biological neuron is a finite precision machine, the total effect of a set of spikes on the soma is almost linear in their individual effects when such effects are small ($\approx \frac{\epsilon}{C(m+1)}$), and owing to the exponential nature of the decay of the effects of afferent as well as efferent spikes and the existence of a refractory period, a quantity $\mu < 1$ can be computed such that the residual effect of the afferent spikes that have arrived at a synapse, whose effects on the soma have decayed below $\frac{\epsilon}{C(m+1)}$ (and that of the efferent spikes of the neuron satisfying the same constraint) is bounded from above by the infinite series $\frac{\epsilon}{C(m+1)}(1 + \mu + \mu^2 + \cdots + \mu^k + \cdots)$. Setting $C > \frac{1}{1-\mu}$ then guarantees that each such residual is less than $\frac{\epsilon}{(m+1)}$. This argument, in essence, demonstrates that the period of effectiveness of a spike since its impact at a given afferent synapse or departure after being generated at the soma is bounded from above.[3] We model this feature by imposing the following restrictions on P^*:

1. $\forall i = 0, \ldots, m$ and $\forall j, \exists \tau_i$ such that $\forall t \geq \tau_i \; \frac{\partial P^*}{\partial x_i^j} \mid_{x_i^j = t} = 0$ irrespective of the values assigned to the other variables.
2. $\forall i = 0, \ldots, m$ and $\forall j, \forall t \leq 0 \; \frac{\partial P^*}{\partial x_i^j} \mid_{x_i^j = t} = 0$ irrespective of the values assigned to the other variables.
3. $\forall i = 0, \ldots, m$ and $\forall j, P^*(\cdot) \mid_{x_i^j = 0} = P^*(\cdot) \mid_{x_i^j = \tau_i}$ all other variables held constant at any values.

[3] This does not necessarily imply that the neuron has a bounded memory of events. Information can be transferred from input spikes to output spikes during the input spikes' period of effectiveness.

4. $P^*(0|\tau_1, 0|\tau_1, \ldots, 0|\tau_2, 0|\tau_2, \ldots, \ldots, 0|\tau_m, 0|\tau_m, \ldots; 0|\tau_0, 0|\tau_0, \ldots) = 0$. In other words, $P^*(\cdot) = 0$ if $\forall i, j\ x_i^j = 0$ or τ_i.

The first criterion enforces that the sensitivity of $P^*(\cdot)$ to spike x_i^j expires after time τ_i. Hence, if for every i there exists an n_i such that $j > n_i \Rightarrow a_i^j \geq \tau_i$; then $P^*(\vec{a}_1, \vec{a}_2, \ldots, \vec{a}_m; \vec{a}_0) = P^*(\vec{a}'_1, \vec{a}'_2, \ldots, \vec{a}'_m; \vec{a}'_0)$ where each $\vec{a}'_i$ is derived from the corresponding $\vec{a}_i$ by setting all values after index n_i to τ_i. The second criterion results from $P^*(\cdot)$ being C^∞ and $\frac{\partial P^*}{\partial x_i^j} \mid_{x_i^j < 0} = 0$ (a spike that has not yet arrived at an afferent synapse can have no effect on the membrane potential, and a spike that has not yet been generated at the soma cannot elicit a postspike hyperpolarization). The third criterion enforces that all else being equal, the membrane potential at the soma is the same whether an afferent spike has just arrived or its effectiveness has just expired, and in the case of an efferent spike whether it has just been generated or its inhibitory effect on the soma has just expired. The fourth criterion enforces that the resting state of the soma is set at 0.

iv. **Finite dimensionality**. The function characterizing the membrane potential can, as a result, be defined over a finite dimensional space. This is based on the observation that at any afferent synapse $i = 1, \ldots, m$, spikes arrive at intervals bounded from below by r_i (the absolute refractory period of the neuron presynaptic to i), and for $i = 0$ spikes are generated at the soma of the neuron at intervals bounded from below by r_0 (the absolute refractory period of the neuron in question). Consequently, at most $n_i = \lceil \tau_i / r_i \rceil$ variables can have values less than τ_i. Based on iii above, we can define,

$$\begin{aligned} P(x_1^1, \ldots, x_1^{n_1}, x_2^1, \ldots, x_2^{n_2}, \ldots, x_m^1, \ldots, x_m^{n_m}; x_0^1, \ldots, x_0^{n_0}) \\ = P^*(x_1^1, \ldots, x_1^{n_1}, \tau_1, \tau_1, \ldots, x_2^1, \ldots, x_2^{n_2}, \tau_2, \tau_2, \ldots, \ldots, \\ x_m^1, \ldots, x_m^{n_m}, \tau_m, \tau_m, \ldots; x_0^1, \ldots, x_0^{n_0}, \tau_0, \tau_0, \ldots) \end{aligned} \quad (2.1)$$

and use $P(\cdot)$ instead of $P^*(\cdot)$ to represent the current membrane potential.[4]

v. **Threshold and refractoriness**. A simple model is assumed for the generation of a spike at a soma, that is, a spike is generated when

[4] A few technicalities should be mentioned here. The definition of P^* assumes that spikes have been arriving at each synapse and have been leaving the soma since time $t = -\infty$. If the number of spikes on any synapse or the number of efferent spikes is finite over the time $(-\infty, 0)$, a denumerable set of dummy variables can be introduced to extend the function's domain to $\mathbb{R}^\infty$. For any such dummy variable x, $\frac{\partial P^*}{\partial x} = 0$ is consistent with the constraints imposed on P^*.

$P(\cdot) = \mathcal{T}$ and $\frac{dP(\cdot)}{dt} \geq 0$.[5] $\mathcal{T}$ is assumed to be a constant. However, it must be noted that a more general criterion of the form $P(\cdot) = \mathcal{T}(\cdot)$ can be transformed into the form $P(\cdot) = \mathcal{T}$ if the parameters of $\mathcal{T}$ are a subset of those of P.

The above model of the neuron does not insist on a specific membrane potential function, only that the particular function possess certain qualitative properties. By retaining this level of generality, we can pose questions that are more basic, such as, To what extent would the dynamics of a neuronal system be affected if the potential function $P(\cdot)$ were to be replaced by any arbitrary function that is unimodal with respect to all variables, and at the same time satisfies all the constraints (items ii, iii, and v above)? Besides, making a model more specific by resorting to explicit functions is much easier than making it more general.

We must mention here that in spite of the generality of the membrane potential function, this model remains some distance from an accurate depiction of the biological neuron. Changes in the strength of synapses, which would translate into evolving potential functions, are not modeled. The biophysical processes that are involved in synaptic modulation are not yet completely understood and the phenomenon continues to inspire intense research. Furthermore, persistent currents such as those that give rise to plateau potentials cannot be modeled in this framework. We can only hope that not much is lost in terms of the salient behavior of the system at our leaving out such details.

3 The Phase-Space

We begin by revising certain definitions for the purpose of instituting the measure of uniformity necessary for the construction of a phase-space for a system of neurons. Previously, x_i^j's for $i = 1, \ldots, m$ represented the time since the arrival of spikes at synapses, and for $i = 0$ the time since the inception of spikes at the soma. We eliminate the asymmetry in the choice of origins of the two sets of variables by redefining x_i^j $\forall i, j$ to represent the time since the inception of the spike at the corresponding soma. The subscript i in x_i^j is now set to refer to a neuron rather than a synapse. In addition to changes in $P(\cdot)$, this prompts a shift in focus from the postsynaptic to the presynaptic neuron.

Given a system of neurons, an upper bound on the number of effective, efferent spikes that a neuron can possess at any time is first computed

[5] $P(\cdot)$ being C^∞, the postspike hyperpolarization cannot be instantaneous. $P(\cdot) = \mathcal{T}$ is crossed twice—once when the spike is generated and once when the inhibitory effect of the spike kicks in. The constraint $\frac{dP(\cdot)}{dt} = \sum_{i,j} \frac{\partial P(\cdot)}{\partial x_i^j} \frac{dx_i^j}{dt} \geq 0$ ensures that the neuron does not spike during the membrane potential's downward journey.

as follows. Let $i = 1, \ldots, \mathcal{S}$ denote the set of all neurons in the system, $k_i = 1, \ldots, m_i$ the set of efferent synapses on neuron i (synapses to which neuron i is presynaptic), $\lambda^i_{k_i}$ the time it takes for a spike generated at the soma of neuron i to reach synapse k_i, $\tau^i_{k_i}$, as before, the time interval over which a spike impinging on synapse k_i is effective on the corresponding postsynaptic neuron, and r_i the absolute refractory period of neuron i. Since its inception, the maximum time until which any spike can be effective on any corresponding postsynaptic neuron is then given by $\chi = \max_{i=1,k_i=1}^{\mathcal{S},m_i}\{\lambda^i_{k_i} + \tau^i_{k_i}\}$. Let ς denote the maximum time period over which any spike is effective on the neuron that generates it, and let $\Upsilon = \max\{\chi, \varsigma\}$. Then $n_i = \lceil \Upsilon / r_i \rceil$ provides an upper bound on the number of effective spikes that neuron i can possess at any time.

The requisite changes in $P(\cdot)$ are threefold. First, the number of variables associated with some synapses is increased so that all synapses actuated by neuron i are consistently assigned n_i variables. This is achieved by setting appropriately fewer variables in $P^*(\cdot)$ to $\tau^i_{k_i}$ in criterion iv of the previous section. Next, $P(\cdot)$ is translated along all but one set of axes such that the former origin is now at $\langle \lambda^{i_1}_{k_{i_1}}, \lambda^{i_1}_{k_{i_1}}, \ldots, \ldots, \lambda^{i_m}_{k_{i_m}}, \lambda^{i_m}_{k_{i_m}}, \ldots, 0, 0, \ldots \rangle$, where $i_1, \ldots, i_m$ are the neurons presynaptic to the neuron in question (i_0) at synapses $k_{i_1}, \ldots, k_{i_m}$. $\frac{\partial P}{\partial x^j_{k_i}} \mid_{x^j_{k_i}=t} = 0$ for $0 \leq t \leq \lambda^i_{k_i}$ holds owing to the manner in which $P(\cdot)$ was previously defined. Finally, references to synapses in the variables are switched to references to appropriate neurons, and multiple variables referencing the same spike (occurs when a neuron makes multiple synapses on a postsynaptic neuron) are consolidated.

We note immediately that the state of a system of neurons can be specified completely by enumerating, for all neurons $i = 1, \ldots, \mathcal{S}$, the positions of the n_i (or fewer) most recent spikes generated by neuron i within Υ time from the present. On the one hand, such a record specifies the exact location of all spikes that are still situated on the axons of respective neurons, and on the other, combined with the potential functions, it specifies the current state of the soma of all neurons. While it is assumed here that neurons do not receive external input, incorporating such is merely a matter of introducing additional neurons whose state descriptions are identical to that of the external input.

This gives us the following initial representation of the state information contributed by each neuron toward the specification of the state of the system: at any given moment neuron i reports the n_i-tuple $\langle x^1_i, x^2_i, \ldots, x^{n_i}_i \rangle$, where each x^j_i denotes the time since the inception of a distinct member of the n_i most recent spikes generated at the soma of neuron i within Υ time from the present. Since n_i is merely an upper bound on the number of such spikes, it is conceivable that fewer than n_i spikes satisfy the criterion, in which case the remaining components in the n_i-tuple are set at Υ. From a dynamical perspective, this amounts to the value of a component growing

until Υ is reached, at which point the growth ceases. The phase-space for neuron i is then the closed n_i-cube $[0, \Upsilon]^{n_i} \subset \mathbb{R}^{n_i}$.

This initial formulation of the phase-space is, however, fraught with redundancy. First, the finite description of the state of a neuron requires that a variable be reused to represent a new spike when the effectiveness of the old spike it represented terminates. Since a variable set at Υ (ineffective spike) is first set to 0 when assigned to a new spike, one of the two positions is redundant. The abstract equivalence of the positions then dictates that Υ be identified with 0. Second, if $\langle x_i^1, x_i^2, \ldots, x_i^{n_i} \rangle$ and $\langle y_i^1, y_i^2, \ldots, y_i^{n_i} \rangle$ are two n_i-tuples that are a nontrivial permutation of one another ($\exists\sigma$, a permutation, such that $\forall j = 1, \ldots, n_i \; x_i^j = y_i^{\sigma(j)}$), then while $\vec{x}_i$ and $\vec{y}_i$ are two distinct points in $[0, \Upsilon]^{n_i}$, they represent the same state of the neuron (which variable represents a spike is immaterial). This stipulates that all permutations of an n_i-tuple be identified with the same state.

In what follows we construct a differentiable manifold that satisfies both of these criteria. The construction is divided into two stages. The first stage transforms the interval $[0, \Upsilon]$ into the unit circle S^1 (spikes now being represented as complex numbers of unit modulus), and the second computes a complex polynomial whose roots identically match this set of complex numbers. By retaining only the coefficients of this polynomial, all order information is eliminated.

Stage 1. We impose on the manifold $\mathbb{R}$ the equivalence relation: $x \sim y$ if $(x - y) = a\Upsilon$, where $x, y \in \mathbb{R}$, and $a \in \mathbb{Z}$, and regard $\mathbb{R}/\sim$ with its standard quotient topology. The equivalence class mapping $\pi\colon \mathbb{R} \to \mathbb{R}/\sim$ can be identified with $\pi(t) = e^{\frac{2\pi i t}{\Upsilon}}$. π maps $\mathbb{R}/\sim$ onto $S^1 = \{z \in \mathbb{C} \mid |z| = 1\}$.

We therefore apply the transformation $\langle x^1, x^2, \ldots, x^n \rangle \to \langle e^{\frac{2\pi i x^1}{\Upsilon}}, e^{\frac{2\pi i x^2}{\Upsilon}}, \ldots, e^{\frac{2\pi i x^n}{\Upsilon}} \rangle$ to the initial formulation of the phase-space of a neuron. The new phase-space is T^n the *n-torus*.

We assume hereafter that all variables x_i^j are normalized, that is, scaled from $[0, \Upsilon]$ to $[0, 2\pi]$. $P(\cdot)$ is also assumed to be modified to reflect the scaling of its domain.

Stage 2. That the set G=$\{\sigma \mid \sigma$ is a permutation of n elements$\}$ forms a Group motivates the approach that the orbit space T^n/G of the action of G on T^n be considered. G, however, does not act freely[6] on T^n, and therefore the quotient topology of T^n/G does not inherit the locally Euclidean structure of T^n. Hence, we explicitly construct the space as a subset of the Euclidean space and endow it with the standard topology. While such a subset necessarily contains boundaries, the construction does shed light on the intrinsic structure of the space.

[6] A Group G acts freely on a set X if $\forall x$ ($gx = x$ implies $g = e$).

As noted earlier, we apply the transformation $\langle z_1, z_2, \ldots, z_n \rangle \rightarrow \langle a_n, a_{n-1}, \ldots, a_0 \rangle$ where $a_n, a_{n-1}, \ldots, a_0 \in \mathbb{C}$ are the coefficients of $f(z) = a_n z^n + a_{n-1} z^{n-1} + \cdots + a_0$ whose roots lie at $z_1, z_2, \ldots, z_n \in \mathbb{C}$. The immediate question, then, is what are necessary and sufficient constraints on $\langle a_n, a_{n-1}, \ldots, a_0 \rangle \in \mathbb{C}^{n+1}$ for all roots z_i of $f(z)$ to satisfy $|z_i| = 1$. We answer this in two steps. First, we consider the case of distinct roots, and subsequently that of multiple roots.

Theorem 1. *Let $f(z) = a_n z^n + a_{n-1} z^{n-1} + \cdots + a_1 z + a_0$ be a complex polynomial of degree n:*

- *Let $f^*(z)$ be defined as $f^*(z) = z^n \bar{f}(1/z) = \bar{a}_0 z^n + \bar{a}_1 z^{n-1} + \cdots + \bar{a}_n$, where $\bar{a}_i$ represents the complex conjugate of a_i.*
- *Construct the sequence $\langle f_0(z), f_1(z), \ldots, f_{n-1}(z) \rangle$ as follows:*
  - *i. $f_0(z) = f'(z)$ where $f'(z)$ is the derivative of $f(z)$, and*
  - *ii. $f_{j+1}(z) = \bar{b}_0^{(j)} f_j(z) - b_{n-1-j}^{(j)} f_j^*(z)$ for $j = 0, 1, \ldots, n-2$, where $f_j(z)$ is represented as the polynomial $\sum_{k=0}^{n-1-j} b_k^{(j)} z^k$.*

In each polynomial $f_j(z)$, the constant term $b_0^{(j)}$ is a real number, which we denote by δ_j: $\delta_{j+1} = b_0^{(j+1)} = |b_0^{(j)}|^2 - |b_{n-1-j}^{(j)}|^2$ for $j = 0, 1, \ldots, n-2$.

Then, necessary and sufficient conditions for all roots of $f(z)$ to be distinct and to lie on the unit circle, $|z| = 1$, assuming without loss of generalization that $a_n = 1$, are:

$$|a_0| = 1, \quad \text{and} \quad a_i = \bar{a}_{n-i} a_0 \quad \text{for} \quad i = 1, 2, \ldots, n-1, \quad \text{and} \tag{3.1}$$

$$\delta_1 < 0 \quad \text{and} \quad \delta_j > 0 \quad \text{for} \quad j = 2, 3, \ldots, n-1. \tag{3.2}$$

Proof. See appendix A.

Stated informally, equations 3.1 ensure that the degree of freedom reflected in the dimensionality of the initial space does not change after the transformation. Of the coefficients $\langle a_{n-1}, a_{n-2}, \ldots, a_0 \rangle$ ($a_n = 1$ w.l.o.g), (i) a_0 has one degree of freedom ($|a_0| = 1$) and (ii) if n is odd, $\langle a_{\lceil n/2 \rceil - 1}, \ldots, a_1 \rangle$ can be derived from $\langle a_{n-1}, \ldots, a_{\lceil n/2 \rceil}; a_0 \rangle$ or (iii) if n is even, $a_{\lceil n/2 \rceil}$ has only one degree of freedom ($a_{\lceil n/2 \rceil} = \bar{a}_{\lceil n/2 \rceil} a_0$ implies that $\angle a_{\lceil n/2 \rceil} = (1/2)\angle a_0$) and $\langle a_{\lceil n/2 \rceil - 1}, \ldots, a_1 \rangle$ can be derived from $\langle a_{n-1}, \ldots, a_{\lceil n/2 \rceil + 1}; a_0 \rangle$. Hence, if n is odd, $\langle a_{n-1}, \ldots, a_{\lceil n/2 \rceil}; a_0 \rangle \in \mathbb{C}^{\lfloor n/2 \rfloor} \times S^1$ completely specifies the polynomial, and if n is even, $\langle a_{n-1}, \ldots, a_{\lceil n/2 \rceil + 1}; a_{\lceil n/2 \rceil}, a_0 \rangle \in \mathbb{C}^{\lfloor n/2 \rfloor - 1} \times \mathbb{M}^2$ does the same. $\mathbb{M}^2$ denotes the two-dimensional Möbius band and we shall demonstrate that when n is even, $\langle a_{\lceil n/2 \rceil}, a_0 \rangle \in \mathbb{M}^2$.

$(1/2)\angle a_0$ has two solutions, θ and $(\theta + \pi)$, where $\theta \in [0, \pi)$. $\langle a_{\lceil n/2 \rceil}, a_0 \rangle$ is represented as $\langle \pm |a_{\lceil n/2 \rceil}|, \angle a_0 \rangle$, where $a_{\lceil n/2 \rceil}$'s choice between θ and $(\theta + \pi)$ is transferred to the sign of $|a_{\lceil n/2 \rceil}|$ (positive $|a_{\lceil n/2 \rceil}|$ implies θ and negative

$|a_{\lceil n/2 \rceil}|$ implies $(\theta + \pi)$). Topological constraints then require that all points $\langle \pm|a_{\lceil n/2 \rceil}|, \angle a_0 \rangle \equiv \langle \alpha, 0 \rangle$ be identified with $\langle \pm|a_{\lceil n/2 \rceil}|, \angle a_0 \rangle \equiv \langle -\alpha, 2\pi \rangle$.

Expressions 3.2 enforce $(n-1)$ additional constraints expressed as strict inequalities on C^∞ functions over the transformed space ($\mathbb{C}^{\lfloor n/2 \rfloor} \times S^1$ or $\mathbb{C}^{\lfloor n/2 \rfloor - 1} \times \mathbb{M}^2$). That the functions are C^∞ is evident from their being composed entirely of operators $+$, $-$, $\times$, and $\bar{}$. We note immediately, based on continuity and strict inequality, that the resulting space is open in $\mathbb{C}^{\lfloor n/2 \rfloor} \times S^1$ (n is odd) or $\mathbb{C}^{\lfloor n/2 \rfloor - 1} \times \mathbb{M}^2$ (n is even). Moreover, since the space is the image of a connected set under a continuous mapping, it is connected as well. We denote the resultant space by $\mathbb{L}_n$.

We now consider the case wherein both distinct and multiple roots are allowed.

Theorem 2. *The transformed space corresponding to $f(z)$ constrained to have all roots on $|z| = 1$ without the requirement that they be distinct, is the* closure *of $\mathbb{L}_n$ ($\overline{\mathbb{L}}_n$) in $\mathbb{C}^{\lfloor n/2 \rfloor} \times S^1$ for odd n, or in $\mathbb{C}^{\lfloor n/2 \rfloor - 1} \times \mathbb{M}^2$ for even n. Furthermore, the set $(\overline{\mathbb{L}}_n \backslash \mathbb{L}_n)$ lies on the boundary of $\overline{\mathbb{L}}_n$.*

Proof. See appendix A.

The multidimensional boundary set $(\overline{\mathbb{L}}_n \backslash \mathbb{L}_n)$ can be partitioned, based on the multiplicity of corresponding roots, into connected sets of fixed dimensionality. Each such set is diffeomorphic to an appropriate manifold $\mathbb{L}_{n-1}, \mathbb{L}_{n-2}, \ldots,$ or $\mathbb{L}_0$ by way of the mapping that disregards all but one member of each multiple root. Finally, $\overline{\mathbb{L}}_n$ is bounded because $\forall i \; |a_i| \leq \binom{n}{i}$.

Corollary 1. *The transformed space is a* compact *manifold with* boundaries*; a subset of the same dimension of $\mathbb{C}^{\lfloor n/2 \rfloor} \times S^1$ if n is* odd *or of $\mathbb{C}^{\lfloor n/2 \rfloor - 1} \times \mathbb{M}^2$ if n is* even.

The nature of the spaces corresponding to dimensions $n = 1, 2, 3$ is best demonstrated in figures. For $n = 1$, the phase-space is the unit circle S^1, for $n = 2$, the Möbius band, and for $n = 3$, a solid torus whose cross-section is a concave triangle that revolves uniformly around its centroid as one travels around the torus. Figure 2a presents the phase-spaces for $n = 1$, 2 and 3.

Finally, the phase-space for the entire neuronal system is the Cartesian product of the phase-spaces of the individual neurons. We shall henceforth denote the phase-space of neuron i by ${}^i\overline{\mathbb{L}}_{n_i}$. $P_i(x_1^1, \ldots, x_1^{n_1}, x_2^1, \ldots, x_2^{n_2}, \ldots, x_m^1, \ldots, x_m^{n_m}; x_i^1, \ldots, x_i^{n_i})$ for all neurons i was assumed to be C^∞ in the previous section. In appendix B we define a corresponding function on the transformed space, $\widetilde{P}_i$: ${}^1\overline{\mathbb{L}}_{n_1} \times {}^2\overline{\mathbb{L}}_{n_2} \times \cdots \times {}^m\overline{\mathbb{L}}_{n_m} \times {}^i\overline{\mathbb{L}}_{n_i} \to \mathbb{R}$, which is C^∞.

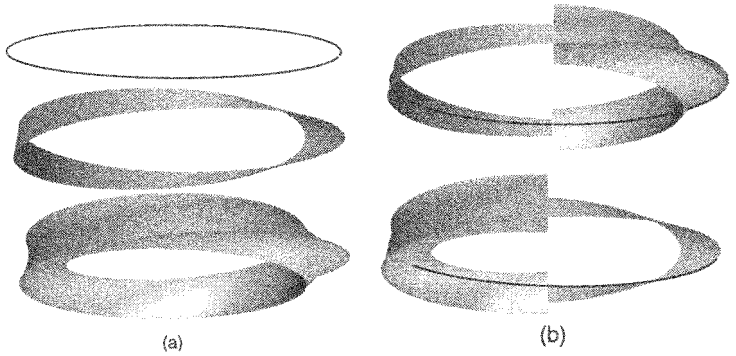

Figure 2: (a) Phase-spaces for $n = 1, 2$ and 3. Note that the one-dimensional boundary of the Möbius band is a circle, and the two- and one-dimensional boundaries of the torus are a Möbius band and a circle, respectively. (b) Subspaces $\sigma \geq 2$ and $\sigma \geq 1$ in the phase-space for $n = 3$. The torus is cut in half, and the circle and the Möbius band within each half are exposed separately.

3.1 Geometric Structure of the Phase-Space: A Finer Topology. In the previous section we constructed the phase-space for an individual neuron as a fixed dimensional manifold, the fixed dimensionality derived from the existence of an upper bound on the number of effective, efferent spikes that the neuron can possess at any time. We also noted that at certain times, the neuron might possess fewer effective spikes. It follows that under such circumstances, the remaining variables are set at $e^{ix_i^j} = 1$. In this section we examine the structure induced in the phase-space as a result of this feature.

Formally, we denote by $p \in \langle {}^1\overline{\mathbb{L}}_{n_1} \times {}^2\overline{\mathbb{L}}_{n_2} \times \cdots \times {}^{\mathcal{S}}\overline{\mathbb{L}}_{n_{\mathcal{S}}} \rangle$ a point in the phase-space and by $\langle p_1, p_2, \ldots, p_{\mathcal{S}} \rangle$ its projection on the corresponding individual spaces, that is, $p_i \in {}^i\overline{\mathbb{L}}_{n_i}$. For each neuron i, we denote the number of variables set at $e^{ix_i^j} = 1$ by σ_i. Such spikes we label as dead since their effectiveness on all neurons has expired. All other spikes we label as live.

To begin, we note that for any ${}^i\overline{\mathbb{L}}_{n_i}$, $Space|_{\sigma_i \geq k} \subset Space|_{\sigma_i \geq (k-1)}$. In the previous section we established that the phase-space of a neuron with a sum total of k spikes is a k-dimensional compact manifold. We now relate a phase-space A corresponding to k spikes to the subset satisfying $\sigma \geq 1$ of a phase-space B corresponding to $(k+1)$ spikes. Equating the appropriate polynomials, $(z-1)[z^k + a_{k-1}z^{k-1} + \cdots + a_0] = z^{k+1} + b_k z^k + \cdots + b_0$, we arrive at

$$b_i = a_{i-1} - a_i \quad \text{for } i = 0, \ldots, k \quad (\text{assuming } a_{-1} = 0, a_k = 1), \quad \text{hence,}$$
$$a_{i-1} = \sum_{j=i}^{k} b_j + 1 \quad \text{for } i = 1, \ldots, k. \tag{3.3}$$

That the mapping $\mathcal{F}_k\colon A \to B, \mathcal{F}_k(a_{k-1}, \ldots, a_{\lceil k/2 \rceil}; \angle a_0) = (b_k, \ldots, b_{\lceil (k+1)/2 \rceil}; \angle b_0)$, is injective follows directly from equations 3.3. That it is an immersion (*rank* $\mathcal{F}_k$ = *dim* $A = k$ at all points) follows from the description of $(D\mathcal{F}_k)$, which when simplified results in the $(k+1 \times k)$ matrix,

$$\begin{pmatrix} I & 0 \\ 0 & C \end{pmatrix} \text{ for } k = \text{even, and } \begin{pmatrix} I \\ D \end{pmatrix} \text{ for } k = \text{odd,} \tag{3.4}$$

where $C = \langle \cos(\frac{\angle a_0}{2}), \sin(\frac{\angle a_0}{2}) \rangle^T$, $D = \langle |a_{\lceil k/2 \rceil}|, 0, 0, \ldots, 2\sin(\frac{\angle a_0}{2}), -2\cos(\frac{\angle a_0}{2}) \rangle$, and I and 0 are identity and zero matrices of appropriate dimensions. A being compact, $\mathcal{F}_k\colon A \to B$ is also an imbedding. Consequently, A is a homeomorphism onto its image; the topology induced by A on $\mathcal{F}_k(A)$ is compatible with the subspace topology induced by B on $\mathcal{F}_k(A)$. Finally, repeated application of the argument establishes that $\forall k\, Space|_{\sigma \geq k}$ is a regular submanifold of $Space|_{\sigma \geq (k-1)}$.

Alternatively, the mapping from a space A corresponding to k spikes, to the subset satisfying $\sigma \geq (l-k)$ of a space B corresponding to l spikes, can be constructed directly by composing multiple $\mathcal{F}$'s. Not only does $\mathcal{F}_k^l = \mathcal{F}_{l-1} \circ \mathcal{F}_{l-2} \circ \cdots \circ \mathcal{F}_k$ map A into B, but it also maps relevant subspaces[7] of A into corresponding subspaces of B. Since $(D\mathcal{F}_k^l) = (D\mathcal{F}_{l-1}) * (D\mathcal{F}_{l-2}) * \cdots * (D\mathcal{F}_k)$, it follows from the arguments in the previous paragraph that $\mathcal{F}_k^l$ is an imbedding.

Figure 2b displays the subspaces satisfying $\sigma \geq 2$ (imbedding of a circle) and $\sigma \geq 1$ (imbedding of a Möbius band) located within the phase-space for $n = 3$. We shall henceforth denote by ${}^i\overline{\mathbb{L}}_{n_i}^j$ the subspace satisfying $\sigma_i \geq j$ for neuron i. Consequently, ${}^i\overline{\mathbb{L}}_{n_i} = {}^i\overline{\mathbb{L}}_{n_i}^0 \supset {}^i\overline{\mathbb{L}}_{n_i}^1 \supset \cdots \supset {}^i\overline{\mathbb{L}}_{n_i}^{n_i}$.

It must be noted that $\mathcal{F}_k^l\colon A \to B$ not only maps phase-spaces but also maps flows identically, a fact manifest in the following informal description of the dynamics of the system: If the state of the system at a given instant is such that neither any live spike is on the verge of death nor is any neuron on the verge of spiking, then all live spikes continue to age uniformly. If a spike is on the verge of death, it expires (i.e., stops aging). This occurs when a spike reaches $e^{ix_i^j} = 1$. If a neuron is on the verge of spiking, exactly one dead spike corresponding to that neuron is turned live.

Since all dead spikes remain stationary at $e^{ix_i^j} = 1$, they register as a constant factor in the dynamics of a neuron. This has the important ramification that the total number of spikes assigned to a neuron has little impact on its phase-space dynamics. $\mathcal{F}_k^l\colon A \to B$, in essence, constitutes a bridge between all flows that correspond to a given number of live spikes pos-

[7] Subspaces corresponding to at most $(k-1), (k-2), \ldots, 0$ live spikes.

sessed by a neuron over a given interval of time. While the total number of spikes assigned to a neuron dictates the dimensionality of its entire phase-space, flows corresponding to a given number of live spikes lie on a fixed dimensional submanifold and are C^∞-conjugate[8] to each other.

We note that $\forall j \geq 1$ ${}^i\overline{\mathbb{L}}^j_{n_i}$ is a C^∞ hypersurface of dimension $(n_i - j)$ in ${}^i\overline{\mathbb{L}}_{n_i}$.[9] Moreover, since $\forall j \geq 2$ ${}^i\overline{\mathbb{L}}^j_{n_i}$ features a multiple root at e^{i0}, it lies on the boundary of ${}^i\overline{\mathbb{L}}_{n_i}$.

The submanifolds ${}^i\overline{\mathbb{L}}^j_{n_i}$ $(j = 1, \ldots, n_i)$ are not revealed in the topology of ${}^i\overline{\mathbb{L}}_{n_i}$ regarded (as the case may be) as a subspace of $\mathbb{C}^{\lfloor n_i/2 \rfloor} \times S^1$ or of $\mathbb{C}^{\lfloor n_i/2 \rfloor - 1} \times \mathbb{M}^2$ (topologized by respective standard differentiable structures). We therefore assign ${}^i\overline{\mathbb{L}}_{n_i}$ the topology generated by the family of all relatively open subsets of ${}^i\overline{\mathbb{L}}^j_{n_i}$, $\forall j \geq 0$. This new, strictly finer topology better matches our intuitions about the set of states that should comprise the neighborhood of any given state of the system.

In the previous section we defined a C^∞ function $\widetilde{P}_i(\cdot)$ that represented the potential at the soma of neuron i. We denote by P^S_i the subset of the space wherein $\widetilde{P}_i(\cdot) = \mathcal{T}$, and by P^I_i the subset wherein $d\widetilde{P}_i(\cdot)/dt \geq 0$ is additionally true. Trivially then, $P^I_i \subseteq P^S_i$. Based on the implicit function theorem and the fact that at all points satisfying $\widetilde{P}_i(\cdot) = \mathcal{T}$ there exists a direction x such that $\partial\widetilde{P}_i(\cdot)/\partial x \neq 0$,[10] it follows that P^S_i is a C^∞ regular submanifold of codimension 1. Moreover, P^I_i is a closed subset of P^S_i since $\widetilde{P}_i(\cdot)$ being C^∞, $d\widetilde{P}_i(\cdot)/dt$ along any direction d/dt is C^∞ on P^S_i.

4 The Velocity Field

In this section we stipulate the velocity field, $\mathcal{V}$: $\prod_{i=1}^{\mathcal{S}} {}^i\overline{\mathbb{L}}_{n_i} \rightarrow \prod_{i=1}^{\mathcal{S}} T({}^i\overline{\mathbb{L}}_{n_i})$, that arises from the natural dynamics of the system. $T(\cdot)$ denotes the tangent bundle (appropriated from the ambient space $\mathbb{C}^{\lfloor n_i/2 \rfloor} \times S^1$ or $\mathbb{C}^{\lfloor n_i/2 \rfloor - 1} \times \mathbb{M}^2$).

We define two vector fields, $\mathcal{V}^1$ and $\mathcal{V}^2$. For the case in which no spike is on the verge of death and no neuron is on the verge of spiking, the velocity is specified by $\mathcal{V}^1$. Formally, $\mathcal{V}^1$ applies to all points $p \in \prod_{i=1}^{\mathcal{S}} ({}^i\overline{\mathbb{L}}^{\sigma_i}_{n_i} \setminus {}^i\overline{\mathbb{L}}^{\sigma_i+1}_{n_i})$ for all values of $\sigma_i \leq n_i$ that satisfy $\forall i = 1, \ldots, \mathcal{S}$ $p \notin P^I_i$. For the case in which a neuron is on the verge of spiking, the velocity is specified by $\mathcal{V}^2$. Formally, $\mathcal{V}^2$ applies to all points p that satisfy $\exists i$ such that $p \in P^I_i$. Since $\mathcal{V}^1$

[8] Since $\mathcal{F}^l_k$: $A \rightarrow B$ is C^∞.

[9] $S \subset M$ is a k-dimensional C^p hypersurface in the m-dimensional manifold M if for every point $s \in S$ and coordinate neighborhood $\langle U, \phi \rangle$ of M such that $s \in U$, $\phi(U \cap S)$ is the *image* of an open set in $\mathbb{R}^k$ under an injective C^p mapping of rank k, φ: $\mathbb{R}^k \rightarrow \mathbb{R}^m$.

[10] This is not the case when $\widetilde{P}_i(\cdot) = \mathcal{T}$ is a point. In all other cases there exist effective spikes that satisfy the criterion.

is, by definition, a function of σ_i's for all $i = 1, \ldots, \mathcal{S}$, it accounts for the case in which a spike is on the verge of death.

It follows from the natural dynamics of the system that given any point $p = \langle p_1, \ldots, p_{\mathcal{S}} \rangle$ in the phase-space, $\mathcal{V}^1(p) = \langle \mathcal{V}_1^1(p), \ldots, \mathcal{V}_{\mathcal{S}}^1(p) \rangle$ can be defined as $\langle \mathcal{V}_1^1(p_1), \ldots, \mathcal{V}_{\mathcal{S}}^1(p_{\mathcal{S}}) \rangle$. That is, each component $\mathcal{V}_i^1$ of $\mathcal{V}^1$ is solely a function of $p_i \in {}^i\overline{\mathbb{L}}_{n_i}^{\sigma_i}$. This is also true for $\mathcal{V}^2$. Once it is determined which P_i^I's p lies on, each component $\mathcal{V}_i^2$ can be computed based solely on p_i.

We noted earlier that the differentiable structures of ${}^i\overline{\mathbb{L}}_{(n_i-\sigma_i)}^0$ and ${}^i\overline{\mathbb{L}}_{n_i}^{\sigma_i}$ are compatible by virtue of $\mathcal{F}_{(n_i-\sigma_i)}^{n_i}$ being an imbedding. We also noted that flows corresponding to $\mathcal{V}^1$ for k live spikes lie on a k-dimensional submanifold and are C^∞-conjugate to each other, $\mathcal{F}_k^l$ constituting the bridge between such flows. We therefore define $\mathcal{V}_i^1$ on $({}^i\overline{\mathbb{L}}_{(n_i-\sigma_i)}^0 \backslash {}^i\overline{\mathbb{L}}_{(n_i-\sigma_i)}^1)$. The corresponding velocity field on $({}^i\overline{\mathbb{L}}_{n_i}^{\sigma_i} \backslash {}^i\overline{\mathbb{L}}_{n_i}^{\sigma_i+1})$ is then defined as $\mathcal{F}_{(n_i-\sigma_i)\star}^{n_i}(\mathcal{V}_i^1)$.[11]

Let p_i correspond to $z^{n_i-\sigma_i} + a_{n_i-\sigma_i-1} z^{n_i-\sigma_i-1} + \cdots + a_0 = \prod_{j=1}^{n_i-\sigma_i}(z - z_j)$. Since all roots rotate at constant speed, that is, $z_j = e^{i(\theta_j + \frac{2\pi t}{\Upsilon})}$, $dz_j/dt = \frac{2\pi i}{\Upsilon} z_j$. Simple algebra then demonstrates:

Theorem 3. *$\mathcal{V}_i^1$ for the C^∞-conjugate flows on $({}^i\overline{\mathbb{L}}_{(n_i-\sigma_i)}^0 \backslash {}^i\overline{\mathbb{L}}_{(n_i-\sigma_i)}^1)$ is given by*

$$\frac{da_{n_i-\sigma_i-k}}{dt} = \frac{2\pi}{\Upsilon} k\hat{\theta} \text{ for } k = 1, \ldots, \left\lfloor \frac{n_i - \sigma_i}{2} \right\rfloor \text{ and } k = n_i - \sigma_i \tag{4.1}$$

$$\frac{d|a_{\frac{n_i-\sigma_i}{2}}|}{dt} = 0 \text{ when } (n_i - \sigma_i) \text{ is even.} \tag{4.2}$$

$\hat{\theta}$ denotes the basis vector $\partial/\partial\theta$ on $\mathbb{C} \ni a_{n_i-\sigma_i-k}$ for any $k = 1, \ldots, \lfloor \frac{n_i-\sigma_i}{2} \rfloor$, represented as $\{\langle r, \theta \rangle \mid re^{i\theta} = a_{n_i-\sigma_i-k}\}$, on $S^1 \ni a_0$ represented as $\{\theta \mid \theta = \angle a_0\}$, and on $\mathbb{M}^2 \ni \langle a_{\frac{n_i-\sigma_i}{2}}, a_0 \rangle$ for even $(n_i - \sigma_i)$, represented as $\{\langle r, \theta \rangle \mid r = \pm|a_{\frac{n_i-\sigma_i}{2}}|, \theta = \angle a_0\}$.

Stated informally, each parameter revolves around its origin at uniform speed, the speed of successive parameters increasing in steps of $(2\pi/\Upsilon)$. Turning our attention to $\mathcal{V}_i^2$, we note that $\mathcal{V}_i^2(p_i)$ can be obtained from $\mathcal{V}_i^1(p_i)$ by setting σ_i to $(\sigma_i - 1)$; $\mathcal{V}_i^2(p_i)$ for $p_i \in ({}^i\overline{\mathbb{L}}_{n_i}^{\sigma_i} \backslash {}^i\overline{\mathbb{L}}_{n_i}^{\sigma_i+1})$ is equivalent to $\mathcal{V}_i^1(p_i)$ on ${}^i\overline{\mathbb{L}}_{n_i}^{\sigma_i-1}$ ignoring the fact that p_i lies additionally on ${}^i\overline{\mathbb{L}}_{n_i}^{\sigma_i} \subset {}^i\overline{\mathbb{L}}_{n_i}^{\sigma_i-1}$.

We have defined $\mathcal{V}$: $\prod_{i=1}^{\mathcal{S}} {}^i\overline{\mathbb{L}}_{n_i} \to \prod_{i=1}^{\mathcal{S}} T({}^i\overline{\mathbb{L}}_{n_i})$ based on our consummate knowledge of flows in the phase-space. The utility of this construction is to be found in the assistance it renders in the analysis of local properties of

[11] We use the notation, $F_\star(X_p)f = X_p(f \circ F)$ where F is a C^∞ map of manifolds, X_p is a tangent vector at p, and f is an arbitrary function that belongs to $C^\infty(F(p))$.

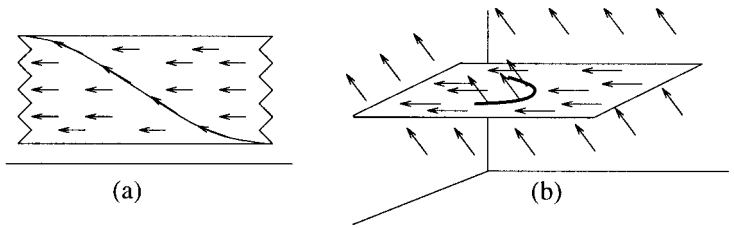

Figure 3: Schematic depiction of the velocity field $\mathcal{V}$.

flows (a topic pursued in the companion article in this issue). $\mathcal{V}$ is however discontinuous. It must therefore be confirmed that $\mathcal{V}$ does not generate inconsistencies in the model. We consider this problem next.

Both $\mathcal{V}_i^1$ and $\mathcal{V}_i^2$ are smooth on $({}^i\overline{\mathbb{L}}_{n_i}^{\sigma_i} \setminus {}^i\overline{\mathbb{L}}_{n_i}^{\sigma_i+1})$ for any σ_i. The only points where the projection of a trajectory $\Psi(x,t)$ on ${}^i\overline{\mathbb{L}}_{n_i}^{\sigma_i}$ is not differentiable (where, incidentally, it is not even continuous) is therefore when it meets ${}^i\overline{\mathbb{L}}_{n_i}^{\sigma_i+1}$ or it meets P_i^I. This gives rise to the potential problem that $d\widetilde{P}_i(\cdot)/dt$ might not be computable on P_i^I, for whereas $\widetilde{P}_i(\cdot)$ is C^∞, one component of $d\Psi(x,t)/dt$ in ${}^i\overline{\mathbb{L}}_{n_i}^{\sigma_i}$—the velocity of the dead spike that just turned live—is undefined. However, one needs only to recall from appendix B that for any spike x stationed at e^{i0}, $\partial P_i(\cdot)/\partial x = 0$ over an infinitesimal interval $(e^{i\delta} > e^{ix} > e^{i(2\pi-\delta)})$. The problem is therefore resolved trivially.

Figure 3 presents a schematic depiction of the velocity field $\mathcal{V}$ described above. Figure 3a displays $\mathcal{V}$ corresponding to a patch of ${}^i\overline{\mathbb{L}}_2^1$ within a patch of ${}^i\overline{\mathbb{L}}_2^0$, and Figure 3b displays $\mathcal{V}$ corresponding to a P_i^I lying on a patch of ${}^i\overline{\mathbb{L}}_3^1$ within ${}^i\overline{\mathbb{L}}_3^0$.

We are now in a position to define an abstract dynamical system without reference to neuronal systems. The phase-space of the system is $\prod_{i=1}^{\mathcal{S}} {}^i\overline{\mathbb{L}}_{n_i}$, which contains $\mathcal{S}$ C^∞ hypersurfaces P_i^I for $i = 1, \ldots, \mathcal{S}$. The velocity field $\mathcal{V}$ on the phase-space is as defined in the previous theorem.

In order for the system to be consistent, each hypersurface P_i^I must at the least satisfy two additional constraints. First, the criterion that any neuron i possess at most n_i live spikes can be enforced by the constraint: $\forall i = 1, \ldots, \mathcal{S}$, $P_i^I \cap (\prod_{j=1}^{i-1} {}^j\overline{\mathbb{L}}_{n_j}^0 \times ({}^i\overline{\mathbb{L}}_{n_i}^0 \setminus {}^i\overline{\mathbb{L}}_{n_i}^1) \times \prod_{j=i+1}^{\mathcal{S}} {}^j\overline{\mathbb{L}}_{n_j}^0) = \emptyset$. Second, the criterion that multiple roots (coincident spikes) occur only at e^{i0} (when the spikes are dead) can be enforced by requiring that the normal to the hypersurface $P_i^I \cap \prod_{j=1}^{\mathcal{S}} ({}^j\overline{\mathbb{L}}_{n_j}^{\sigma_j-1} \setminus {}^j\overline{\mathbb{L}}_{n_j}^{\sigma_j+1})$ at $P_i^I \cap \prod_{j=1}^{\mathcal{S}} ({}^j\overline{\mathbb{L}}_{n_j}^{\sigma_j} \setminus {}^j\overline{\mathbb{L}}_{n_j}^{\sigma_j+1})$ not be orthogonal to $\mathcal{V}^2$ for all values of i and $\sigma_j \leq n_j$.

Finally, since neurons that spike spontaneously are not modeled, one can additionally enforce the weaker constraint: $\forall i = 1, \ldots, \mathcal{S}$, $P_i^I \cap \prod_{j=1}^{\mathcal{S}} {}^j\overline{\mathbb{L}}_{n_j}^{n_j} = \emptyset$.

It then follows that $\prod_{i=1}^{\mathcal{S}} {}^{i}\overline{\mathbb{L}}_{n_i}^{n_i}$, denoting the state of quiescence in the neuronal system, is the sole fixed point of the dynamical system.

5 Model Simulation and Results

A model is worthwhile only to the extent to which it succeeds in emulating the salient behavior of the physical system it models. In this section we therefore investigate by means of simulation the dynamical behavior of the model just described. We have chosen as our target unit a typical column in the neocortex. These neuronal subsystems are ideally suited for our purpose because their configurations (connectivity pattern, distribution of synapses, etc.) fit statistical distributions and they exhibit distinctive patterns of qualitative dynamical behavior.

5.1 General Anatomical and Physiological Characteristics of Neocortical Columns. Extensive information is available about the anatomical and physiological composition of the neocortex (Braitenberg & Schüz, 1991; Shepherd, 1998). While not sharply defined everywhere, neocortical columns have a diameter of approximately 0.5 mm. Intracolumn connectivity is markedly denser than intercolumn connectivity. Whereas inhibitory connections play a prominent role within a column, intercolumn connections are distinctly excitatory. A column contains approximately 10^5 neurons. The number of synapses each neuron makes ranges between 10^3 and 10^4. The probability of a neuron's making multiple synapses on the dendrite of a postsynaptic neuron is fairly low (Braitenberg, 1978). The connectivity between neurons within a column (intracolumn as opposed to thalamic afferents), while having evolved to achieve a specific function, has been experimentally ascertained to fit a statistical distribution (Schüz, 1992). The location of afferent synapses on the collaterals of the neurons has similarly been shown to fit a statistical distribution (Braitenberg & Schüz, 1991).

Neurons in the neocortex can be divided into two main groups: the spiny and the smooth neurons. Spiny neurons can, in general, be subdivided into pyramidal and stellate cells, with pyramidal cells constituting by far the major morphological class. Diversity among smooth neurons is much higher (Peters & Regidor, 1981). Spiny cells receive only Type II (inhibitory) synapses on their cell bodies and both Type I (excitatory) and Type II synapses on their dendrites. They are presynaptic to only Type I synapses. Smooth cells receive both Type I and Type II synapses on their cell bodies and are, in general, presynaptic to Type II synapses (Peters & Proskauer, 1980). Approximately 80% of all neurons in the neocortex are spiny, and the rest are smooth. Both kinds contribute on average to the same number of synapses per neuron.

Axonal ramifications that make local connections range in length between 100 and 400 μm. The speed of propagation of a spike can be estimated at approximately 1 m/s based on the fact that axons within a col-

umn are unmyelinated. Synaptic delays range between 0.3 and 0.5 msec. Consequently, the time interval between the generation of a spike at an axon hillock and its subsequent arrival across a synapse can be estimated to lie between 0.4 and 0.9 msec. Finally, anatomical investigations suggest that dendritic collaterals are seldom longer than two or three space constants.[12]

The past few decades have witnessed numerous investigations into the electrophysiological activity of the cortex. The majority of these studies fall under two categories. The first is the recording of action potentials (spikes), which reflect the output of single cortical neurons with a time resolution of milliseconds, and the second is the recording of the electroencephalogram (EEG), a slow, continuous wave that reflects the activity of hundreds of thousands of neurons.

An aspect shared universally among single cortical neuron recordings is the apparent stochastic nature of the spike trains (Burns & Webb, 1976). A good measure of spike variability is given by the coefficient of variation (CV)[13] of an ISI distribution. Spike trains of cortical neurons have CVs ranging from 0.5 to 1.1, resembling a Poisson process for which CV= 1.

In the case of EEG recordings, the outputs are significantly more abstruse. Classical signal analysis has long considered EEG records as realizations of (often stationary) stochastic processes, and spectral analysis has been the conventional method for extracting the dominant frequencies of the rhythms (Erdi, 1996). Spectral charts of EEG records generally exhibit peak densities at frequencies of major cerebral rhythms, superimposed on a 1/f spectral envelope. Recently, some researchers have come to regard EEG records as the chaotic output of a nonlinear system (Basar, 1990) and have attempted to measure the dimensionality of its various components (Babloyantz, Salazar, & Nicolis, 1985; Röschke & Basar, 1989). Unfortunately, the results remain varied and inconclusive.

5.2 Experimental Setup. We conducted simulation experiments to compare the dynamical characteristics of our model to the salient properties of the dynamics of neocortical columns. The parameterized function $v(x, t) = \{\alpha Q/(x\sqrt{t})\}e^{-\beta x^2/t}e^{-\gamma t}$ was used to model the response to a spike at the soma of a neuron (refer to MacGregor & Lewis, 1977, for a derivation of this equation). The total response at the soma was computed as the sum of the responses to individual spikes. The parameters α, β, and γ were set so as to fit response curves from NEURON v2.0 (Hines, 1993). Refractoriness was modeled by the function $ce^{-\delta t}$.[14]

[12] Distance over which response drops by a factor of e.

[13] The ratio of the standard deviation to the mean of the ISI histogram ($\sigma_{\Delta t}/\overline{\Delta t}$).

[14] Whereas in the abstract model, $P(\cdot)$ must necessarily be C^∞, such restrictions do not apply here because the function is, in any case, discretized in time for simulation.

Four separate sets of experiments were performed. The physiological accuracy of the model was enhanced with each successive set of experiments. In each case a neuronal system comprising 1000 neurons with each neuron connected randomly to 100 other neurons was modeled.[15]

5.2.1 Model I. Eighty percent of all neurons in the system were randomly chosen to be excitatory (spiny) and the rest inhibitory (smooth). The strength of a synapse (Q) was chosen randomly from a uniform distribution over the range [5.7, 15.7]. Values for the parameters α, β, and γ were chosen so as to model a synapse with an uncharacteristically fast response time ($\tau \approx 10$ msec) and were set at fixed values for the entire system. x in $v(x, t)$ was also set at a fixed value for the entire system. In other words, not only were all afferent synapses assumed to be located at the same distance from the soma, but they were also assumed to be generating identical (to a constant factor) responses. Excitatory and inhibitory neurons were constructed to be identical in all respects save the strength of inhibitory synapses, which was enhanced to six times the magnitude ($Q \times 6.0$). The lengths of the axonal collaterals and their variability were assumed to be uncharacteristically large; the time interval between the birth of a spike at a soma and its subsequent arrival across a synapse was randomly chosen to lie between 5 and 15 msec (uniformly distributed). The parameters c and δ in the function modeling refractoriness were set at appropriate values and held constant over the entire system. The threshold was established such that at least 10 excitatory spikes (and no inhibitory spikes) with coincident peak impact[16] were required to cause a neuron to fire and it was held constant over the entire system. The system was initialized with 5 live spikes per neuron chosen randomly over their respective lifetimes (approximately 200 spikes per second per neuron).

5.2.2 Model II. The lengths of the axonal collaterals as well as their variability were modified to reflect realistic dimensions. The time interval between the birth of a spike at a soma and its subsequent arrival across a synapse was randomly chosen to lie between 0.4 and 0.9 msec. All other aspects of the model were left unchanged.

5.2.3 Model III. The unrealistic assumption that all afferent synapses be located at the same distance from the soma and generate similar responses was eliminated. Instead, the locations of the synapses were chosen

[15] Simulating larger systems of neurons was found to be computationally intractable. Instead, we ran experiments on systems with 100 and 500 neurons. The qualitative characteristics of the dynamics described here became more pronounced as the number of neurons in the system (and their connectivity) was increased.

[16] The probability of 10 spikes' arriving in such a manner that their peak impact on a soma coincide is very low. It took on average 20 live spikes to cause a neuron to fire.

based on anatomical data. On the spiny cells, inhibitory synapses were cast randomly to within a distance of 0.3 space constants from the soma, and excitatory synapses were cast randomly from a distance of 0.3 to 3.0 space constants from the soma. On smooth cells, both inhibitory and excitatory synapses were cast randomly between distances of 0.0 and 3.0 space constants from the soma. Since a synapse closer to the soma induced a more intense response, we were also able to eliminate the factitious assumption of inhibitory synapses' being six times stronger than excitatory synapses. Next, 50% of all excitatory synapses were randomly chosen to be of type non-NMDA (AMPA/kainate) and the rest of type NMDA.[17] Likewise, 50% of all inhibitory synapses were randomly chosen to be of type $GABA_A$ and the rest of type $GABA_B$. The characteristic response of each kind of synapse was modeled after graphs reported in Bernander, Douglas, and Koch (1992) using the parameterized potential function. Finally, the threshold for firing of a neuron was reduced to an uncharacteristically low value, and the system was initialized at a very sparsely active state (approximately 20 spikes per second per neuron).

5.2.4 Model IV. The threshold for firing of a neuron was returned to its characteristic value, and the system was initialized at a more realistic state. (Two separate initializations, one with approximately 100 spikes per second per neuron and another with approximately 150 spikes per second per neuron, were considered.)

5.3 Data Recorded. The dynamics of several random instantiations of the models was investigated. In each case neurons were assigned a maximum number of effective spikes ($n = \lceil \Upsilon / r \rceil$) based on upper ($\Upsilon$) and lower ($r$) bounds computed from physiological parameters. Each system was initialized randomly, and the ensuing dynamics was observed in the absence of external input. Two classes of data was recorded. The temporal evolution of the total number of live spikes registered by the entire system (a feature peculiar to the dynamical system under consideration) was recorded as an approximation to EEG data, and individual spike trains of 10 randomly chosen neurons from each system were recorded for comparison with real spike train recordings.

5.4 Results. The most significant outcome of the simulation experiments was the emergence of distinct patterns of qualitative dynamical behavior that were found to be robust across all models and their numer-

[17] While the voltage dependence of NMDA synapses can be modeled in this framework, for the sake of simplicity, the NMDA receptors were assumed to be relieved of the Mg^{2+} block at all times. In other words, they were set at peak conductance irrespective of the postsynaptic polarization.

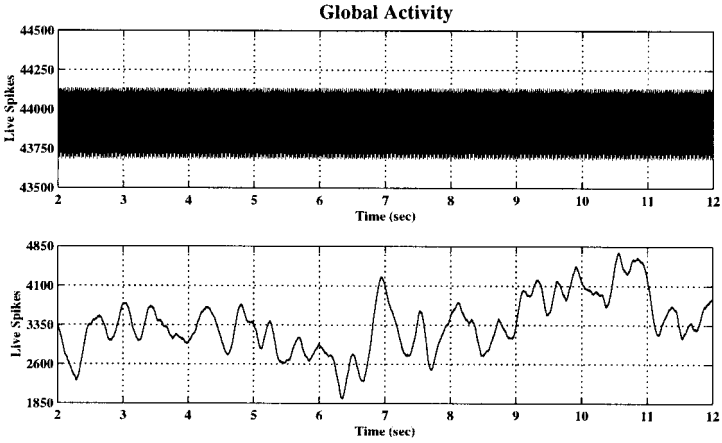

Figure 4: Time series (over the same interval) of the total number of live spikes from a representative system initiated at different levels of activity. Two of the three classes of behavior, intense periodic activity and sustained chaotic activity, are shown.

ous instantiations. Three classes of behavior were encountered. Each randomly generated instantiation of the models possessed an intrinsic range of activity[18] over which the system displayed sustained chaotic behavior. This range was found to conform with what is generally held as normal operational conditions in the neocortex. If the system was initiated at an activity level below this range, the total number of live spikes dropped as the dynamics evolved, until the trivial fixed point of zero activity (the state of quiescence) was reached. In contrast, if the system was initiated at an activity level above this range, the total number of live spikes rose until each neuron spiked periodically at a rate determined primarily by its absolute refractory period. In other words, the system settled into a periodic orbit of intense regular activity resembling a state of seizure. Figure 4 displays the result of one such experiment, a result that is representative of the qualitative dynamics of all the systems that were investigated.

Figures 5 and 6 report results from simulations of systems that were initialized at activity levels within the above-mentioned range. Figure 5 displays normalized time series data pertaining to the total number of live spikes from representative instantiations of each model. Also shown are the results of a power spectrum analysis corresponding to each of the time series.

[18] The corresponding region in the state-space is not exactly quantifiable through numerical analysis because of the nature of chaos. Under conditions of relatively uniform activity, a range with soft bounds was, however, detected with respect to the average spike frequency.

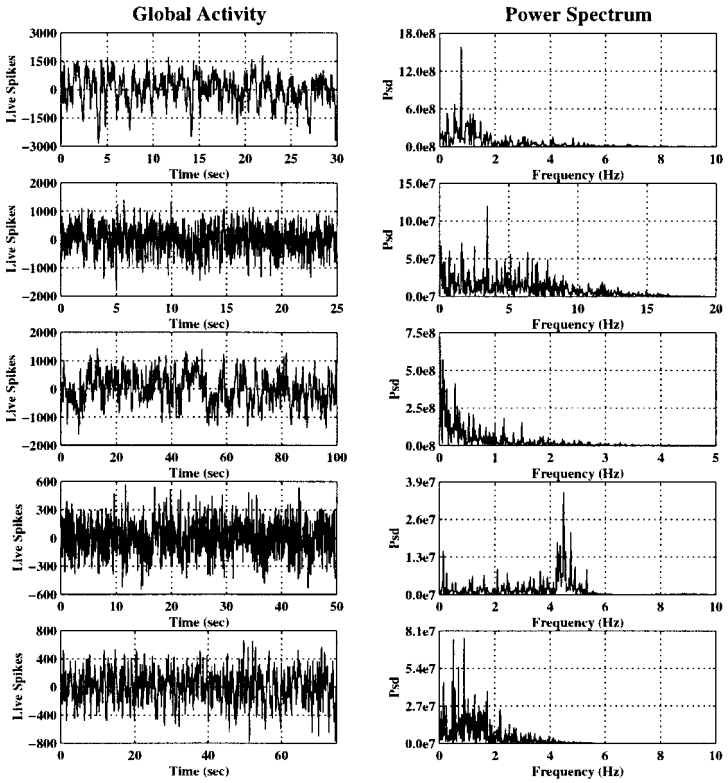

Figure 5: Normalized time series of total number of live spikes from instantiations of each model and corresponding power spectrums.

Although there is a great deal more to an EEG recording than the dynamics of 1000 model neurons, the presence of peak densities at specific frequencies and a 1/f spectral envelope in each of the spectrums supports the view that the abstract system does model the salient aspects of the dynamics of neocortical columns. Furthermore, the absence of any stochastic component to the model[19] demonstrates that the standard features of the EEG spectrum do not necessarily imply that the underlying process is stochastic.

Of the 10 neurons from each system whose spike trains were recorded during simulation, we chose one whose behavior we identified as representative of the mean. Figure 6 displays the time series of ISIs of these neurons (one per model) and their corresponding frequency distributions. The spike

[19] The neurons are deterministic, and the system does not receive external input.

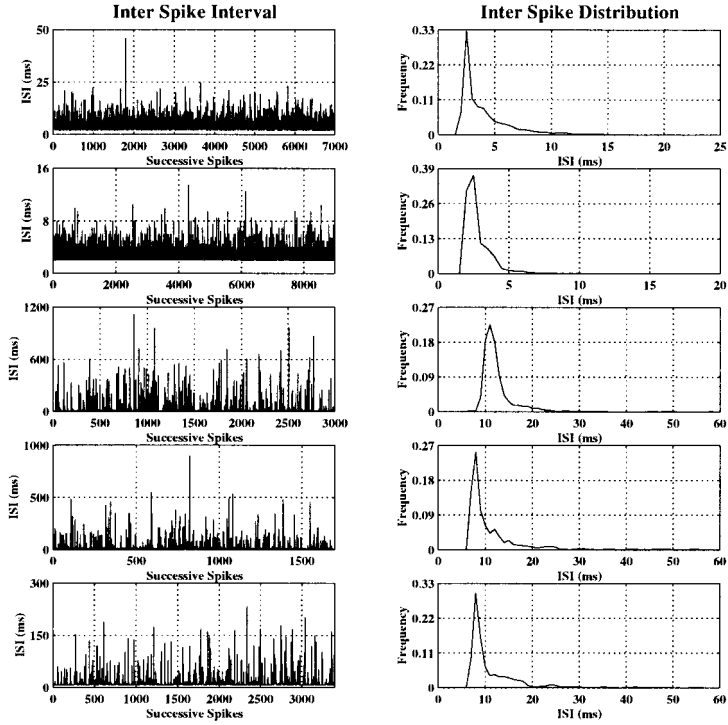

Figure 6: ISI recordings of representative neurons from each model and corresponding frequency distributions.

trains are not only aperiodic, but their ISI distributions suggest that they could be generated from a Poisson process. We also computed the values of the CVs for the various spike trains. The results obtained were encouraging: values ranged from 0.063 to 2.921 with the majority falling around 1.21.[20] Neurons with higher rates of firing tended to have lower values of CV. The agreement between the qualitative aspects of the simulation data and that of real ISI recordings speaks additionally in favor of the viability of our model.

We conducted a second set of experiments to ascertain how predisposed the systems were to the chaotic behavior in the presence of regulating external input. Each system was augmented with two pacemaker neurons—an

[20] Softky and Koch (1993) report that the CVs for spike trains of fast-firing monkey visual cortex neurons lie between 0.5 and 1.1. As the results clearly indicate, our deterministic model can account for this range of data.

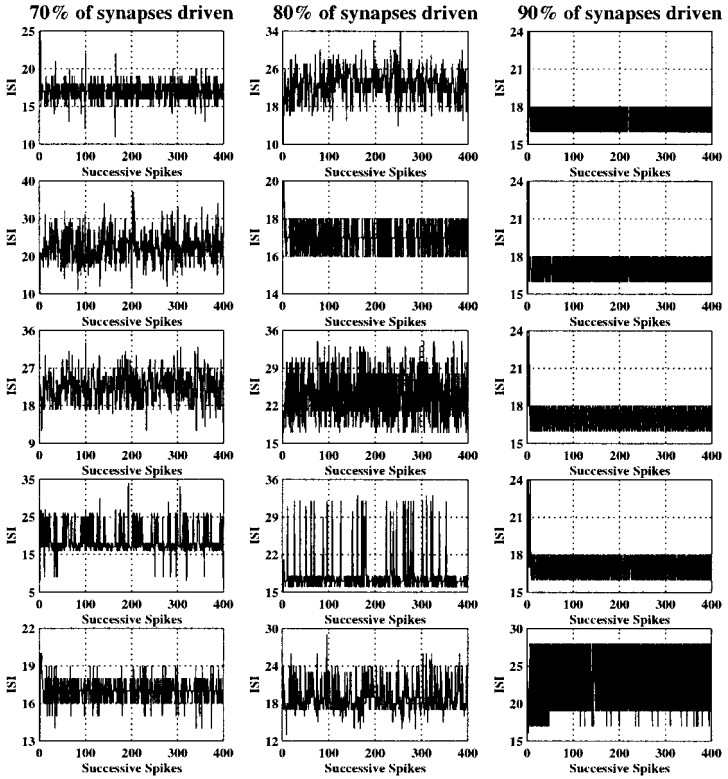

Figure 7: ISI recordings of five representative neurons each, from three systems with 70%, 80%, and 90% of the synapses on neurons driven by two pacemaker cells, are shown.

excitatory and an inhibitory—that spiked at regular intervals.[21] The topology of the system was modified such that of the 100 afferent synapses on each neuron, s received their input from one of the two pacemaker cells chosen randomly, and the remaining $(100 - s)$ received their input from other neurons in the system. s was increased with successive experiments until the system was found to settle into a periodic orbit. Figure 7 depicts the ISIs of five representative neurons each, from systems with s set at 70, 80, and 90. The discovery that the system did not quite settle into a periodic orbit even when 90% of all synapses were driven by periodic spikes bears witness to the system's propensity for chaotic behavior.

[21] The two pacemaker cells spiked every seventeenth time step, generating the simplest form of periodic input.

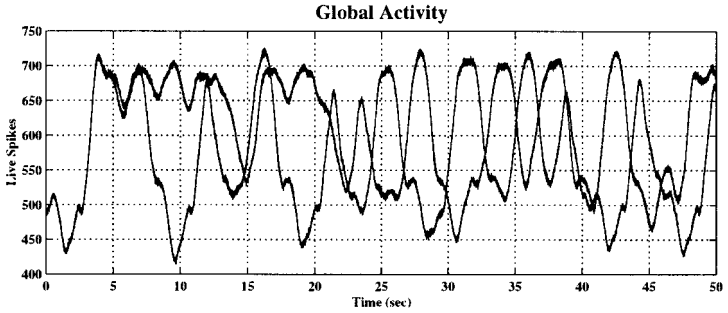

Figure 8: Two trajectories that diverge from very close initial conditions.

Finally, experiments were conducted to determine whether the systems were sensitive to initial conditions, a feature closely associated with chaotic behavior. Each system was initialized at two proximal points in state-space, and the resulting dynamics was recorded. Respective trajectories were found either to diverge strongly or become coincident. Figure 8 depicts the temporal evolution of the total number of live spikes registered by two identical systems of 100 neurons that were initialized with approximately five live spikes per neuron, chosen randomly over respective lifetimes. The initialization of the two systems was identical except for one spike (chosen randomly) in the second system, which was perturbed by 1 msec. As the figure demonstrates, the trajectories diverged strongly.

The results presented in this section are substantially more qualitative than quantitative. The goal of the simulation experiments was not to emulate the dynamics of any specific neocortical column. The data necessary to accomplish such a feat are not available, and we do not claim that the idealized neuron models all aspects of a neocortical neuron. The principal objective of the exercise was to demonstrate that the abstract dynamical system developed in the previous section was capable of modeling adequately the qualitative dynamics of a typical neocortical column. To this end, values for the various parameters were chosen such that the resulting systems resembled generic neocortical columns, and the dynamics of these systems were assessed only to the extent to which they conformed with the generic dynamics of neocortical columns.

6 Conclusions and Future Research

There is general agreement in the scientific community regarding the position that the physical states of the brain are causally implicated in cognition and behavior. What constitutes a discrete brain state is, however, a problem far from resolved.

It is our belief that a principled resolution to the problem can be arrived at by analyzing, exclusively, the dynamics of the brain (or any part thereof) as constrained by its anatomy and physiology. From a dynamical systems perspective, the coherent spatiotemporal structures, if any, inherent in the dynamics of a physical system are revealed in any attractors that are present in its phase-space.

Our objective has therefore been to determine if there exist attractors in the dynamics of systems of neurons and, if so, what their salient characteristics are. The first step in such a program is the construction of an abstract dynamical system that models systems of neurons. We have presented in this article a detailed exposition of one such dynamical system.

In order to determine the viability of the model, we conducted simulation experiments on several instantiations of the system, each modeling a typical column in the neocortex. We found an agreeable fit between the qualitative aspects of the results and that of real data.

A significant outcome of the simulation experiments was the emergence of three distinct categories of qualitative behavior that were found to be robust across all the investigated instantiations of the system. In addition to the trivial behavior of quiescence, the class of systems displayed sustained chaotic behavior in the region of the phase-space associated with normal operational conditions in the neocortex and intense periodic behavior in the region of the phase-space associated with seizure-like conditions in the neocortex.

Based on this evidence, we can surmise that coherent structures do exist in the dynamics of neocortical neuronal systems operating under normal conditions and that they are chaotic attractors. This would then imply that at a certain level, the computational dynamics of such systems is inherently unpredictable. Experimental evidence of the nature presented in this article, however, does not amount to a proof of existence of chaotic attractors in that class of systems. Furthermore, there is as yet little that is known about the structure of these attractors.

In the companion article in this issue, we pursue these issues through a formal analysis of the phase-space dynamics of the abstract system. Not only is the existence of chaos in the noted region of the phase-space confirmed, but also the root cause behind the existence of the distinct categories of qualitative behavior is revealed.

The results of the experiments also shed light on why the strictly neurophysiological perspective to the study of the brain faces profound problems. Whereas the abstract system presented in this article contains a good deal of structure, such is not easily revealed in its dynamics. This is more so in the case of real neurophysiological data, wherein the impression is one of an appalling lack of structure. The incongruence between data recorded at the individual or local neuronal level and at the organism's behavioral level is enormous. Bridging this gap without access to an intermediary model is a formidable task. Whereas approaching the problem via a model might be

deemed weaker because acceptance of the results hinges on the acceptance of the adequacy of the model, it is our view that given the circumstances, this is arguably the only viable approach.

Appendix A

The proof of theorem 1 is based on the following two theorems.

Theorem 4. *All roots of* $f(z)$ *are distinct and lie on* $|z| = 1 \Leftrightarrow$ *(a)* $|a_0| = 1$, $a_i = \bar{a}_{n-i}a_0$ *for* $i = 1, \ldots, n-1$, *and (b)* $f'(z)$ *has all roots in* $|z| < 1$.

Proof.

i. Distinct roots on $|z| = 1 \Rightarrow$ *(a) and (b).* Assume w.l.o.g that $a_n = 1$. z_i is a root of $f(z) \Leftrightarrow z_i^* = (1/\bar{z}_i)$ is a root of $f^*(z)$. $|z_i| = 1$ implies $(1/\bar{z}_i) = z_i$. Hence the roots of $f(z)$ and $f^*(z)$ are identical. Consequently, *a* holds.

That all roots of $f'(z)$ lie in $|z| < 1$ follows from all roots of $f(z)$ being distinct and *Lucas Theorem* (any convex polygon that contains all roots of $f(z)$ also contains all roots of $f'(z)$).

ii. (a) and (b) $\Rightarrow$ *distinct roots on* $|z| = 1$. That the roots of $f(z)$ lie on $|z| = 1$ follows from the following theorem in Cohn (1922).

Lemma 1 (Cohn). *If* $g(z) = b_m z^m + b_{m-1}z^{m-1} + \cdots + b_0$ *satisfies* $b_{m-i} = u\bar{b}_i$ *for all* $i = 0, \ldots, m$ *then* $g(z)$ *has in* $|z| < 1$ *as many roots as* $[g'(z)]^* = z^{m-1}\bar{g}'(1/z)$.

$f(z)$ by criterion a satisfies the premise, and therefore, it has in $|z| < 1$ as many roots as $[f'(z)]^*$. By criterion b $[f'(z)]^*$ has no roots in $|z| < 1$. Hence, f(z) has no roots in $|z| < 1$. Finally, $|a_0| = 1$ constraints all roots of $f(z)$ to lie on $|z| = 1$.

Criterion b then enforces that $f(z)$ has no multiple roots.

Theorem 5. $\delta_1 < 0, \delta_j > 0$ *for* $j = 2, \ldots, n-1$. *(from theorem 1)* $\Leftrightarrow$ *all roots of* $f'(z)$ *lie in* $|z| < 1$.

Proof.

i. $\delta_1 < 0, \delta_j > 0$ *for* $j = 2, \ldots, n-1$. $\Rightarrow$ *all roots of* $f'(z)$ *lie in* $|z| < 1$. Follows directly from the following theorem in Marden (1948).

Lemma 2 (Marden). *If for* $f(z) = a_m z^m + a_{m-1}z^{m-1} + \cdots + a_0$, $\langle f_0(z), f_1(z), \ldots, f_m(z)\rangle$ *is constructed as* $f_j(z) = \sum_{k=0}^{m-j} a_k^{(j)} z^k$ *where* $f_0(z) = f(z)$ *and for* $j = 0, \ldots, m-1$, $f_{j+1}(z) = \bar{a}_0^{(j)} f_j(z) - a_{m-j}^{(j)} f_j^*(z)$, *and* $\delta_{j+1} = a_0^{(j+1)}$ *satisfy* $\delta_1 < 0, \delta_2, \ldots, \delta_m > 0$, *then* $f(z)$ *has all roots in* $|z| < 1$.

ii. All roots of $f'(z)$ *lie in* $|z| < 1 \Rightarrow \delta_1 < 0, \delta_j > 0$ *for* $j = 2, \ldots, n-1$.
(a) $\delta_1 < 0$. *Since* $f'(z) = f_0(z) = b_m z^m + \cdots + b_1 z + b_0$ *(here* $m = n-1$*) has all roots in* $|z| < 1$, *the modulus of the product of all roots is less than 1. Hence,* $|b_0| < |b_m|$, *and* $\delta_1 = |b_0|^2 - |b_m|^2 < 0$.

(b) $\delta_2, \delta_3, \ldots, \delta_{n-1} > 0$ follows from the following theorem in Marden (1948).

Lemma 3 (Marden). *If in lemma 2, $f_j(z)$ has p_j roots in $|z| < 1$ and none on $|z| = 1$ and if $\delta_{j+1} \neq 0$, then $f_{j+1}(z)$ has $p_{j+1} = \frac{1}{2}\{m - j - [(m-j) - 2p_j]sgn\delta_{j+1}\}$ roots in $|z| < 1$ and none on $|z| = 1$.*

$f_0(z) = f'(z)$ has all $n-1$ roots in $|z| < 1$ and none in $|z| = 1$. We have shown that $\delta_1 < 0$. Therefore, $sgn\delta_1 = -1$. Based on the lemma, then, $f_1(z)$ has $p_1 = 0$ roots in $|z| < 1$ and none in $|z| = 1$. In other words, all roots of $f_1(z)$ lie in $|z| > 1$. Using the argument in a, we get, $\delta_2 > 0$. We now apply the lemma repeatedly to get $p_2 = p_1 = 0$ and so on, implying $\delta_3, \ldots, \delta_{n-1} > 0$.

The proof of theorem 2 is based on the following theorem:

Theorem 6. *$x \in \overline{\mathbb{L}_n}$ and $x \notin \mathbb{L}_n \Leftrightarrow x$ denotes a polynomial with all roots on $|z| = 1$ and at least 1 multiple root. $x \in \overline{\mathbb{L}_n}$ and $x \notin \mathbb{L}_n \Rightarrow x$ is a boundary point of $\overline{\mathbb{L}_n}$, that is, every open set containing x contains a $y \notin \overline{\mathbb{L}_n}$.*

Proof.

i. $x \in \overline{\mathbb{L}_n}$ and $x \notin \mathbb{L}_n \Rightarrow$ All roots on $|z| = 1$ and at least 1 multiple root. Since x is a limit point of $\mathbb{L}_n$, $\exists$ denumerable sequence $\langle y_1, y_2, \ldots, y_k, y_{k+1}, \ldots\rangle$, s.t $\forall i\ y_i \in \mathbb{L}_n$ and $\lim_{i\to\infty} y_i = x$. We now apply the following theorem in Coolidge (1908) to the sequence.

Lemma 4 (Coolidge). *If two polynomials $f_1(z) = z^m + a_{m-1}z^{m-1} + \cdots + a_0$ and $f_2(z) = z^m + b_{m-1}z^{m-1} + \cdots + b_0$ are so related that $\forall i\ a_i$ is a constant, and $\forall i\ b_i$ approaches a_i, then the roots of $f_1(z)$ and $f_2(z)$, where each multiple root of order k is counted k times as k roots, may be put into such a one-to-one correspondence that the absolute value of the difference between each two corresponding roots approaches 0.*

Since $x \notin \mathbb{L}_n$, either the corresponding polynomial does not have all roots on $|z| = 1$, or not all roots are distinct. If the first case is true, the distance between at least one set of roots in the theorem is bounded from below, thus contradicting it.

ii. All roots on $|z| = 1$ and at least 1 multiple root $\Rightarrow x \in \overline{\mathbb{L}_n}$ and $x \notin \mathbb{L}_n$. Trivially $x \notin \mathbb{L}_n$. Let $\langle z_1, z_2, \ldots, z_n\rangle$ be the roots of the polynomial corresponding to x with multiple roots of order k repeated k times. Choose a $\delta > 0$ s.t it satisfies $\delta < |(1/2)\min_{\forall i,j\ z_i \neq z_j}(\angle(z_i/z_j))|$. Choose $\langle \delta_1, \delta_2, \ldots, \delta_n\rangle$ s.t $\forall i, j\ i \neq j \Rightarrow \delta_i \neq \delta_j$ and $\forall i,\ 0 < |\delta_i| < \delta$.

Now consider the sequence of ordered sets $\langle z_1 e^{i(\delta_1/2^p)}, z_2 e^{i(\delta_2/2^p)}, \ldots, z_n e^{i(\delta_n/2^p)}\rangle$ for $p = 0, 1, \ldots$. Each set comprises distinct roots on $|z| = 1$. The sequence converges absolutely to $\langle z_1, z_2, \ldots, z_n\rangle$. Since coefficients are continuous functions of roots, the corresponding sequence $\langle y_1, y_2, \ldots, y_k, y_{k+1}, \ldots\rangle$ in coefficient space satisfies $\forall i\ y_i \in \mathbb{L}_n$ and $\lim_{i\to\infty} y_i = x$. x is therefore a limit point of $\mathbb{L}_n$.

iii. $x \in \overline{\mathbb{L}}_n$ *and* $x \notin \mathbb{L}_n \Rightarrow x$ *is a boundary point.* $x \in \mathbb{C}^{\lfloor n/2 \rfloor} \times S^1\,(\mathbb{C}^{\lfloor n/2 \rfloor - 1} \times \mathbb{M}^2)$ $\Rightarrow$ *corresponding polynomial satisfies* $\exists\sigma$, *a permutation, s.t* $z_i = (1/\bar{z}_{\sigma_i})$. *Let* $x \in \overline{\mathbb{L}}_n$ *and* $x \notin \mathbb{L}_n$. *Let* $\langle e^{i\theta_1}, e^{i\theta_2}, \ldots, e^{i\theta_n}\rangle$ *be the set of roots that correspond to* x *and w.l.o.g* $\theta^* = \theta_1 = \theta_2 = \cdots = \theta_k$ $(k \geq 2)$. *For any* $\delta < 1$ *consider the sequence of ordered sets* $\langle((2^p - \delta)/2^p)e^{i\theta^*}, (2^p/(2^p - \delta))e^{i\theta^*}, e^{i\theta_3}, \ldots, e^{i\theta_n}\rangle$ *for* $p = 0, 1, \ldots$ *The sequence converges absolutely to* $\langle e^{i\theta_1}, e^{i\theta_2}, \ldots, e^{i\theta_n}\rangle$, *and each set satisfies* $\exists\sigma$ *s.t* $z_i = (1/\bar{z}_{\sigma_i})$. *Based on arguments identical to ii above, the corresponding sequence* $\langle y_1, y_2, \ldots, y_k, y_{k+1}, \ldots\rangle$ *in coefficient space satisfies* $\forall i\ y_i \notin \overline{\mathbb{L}}_n$ *and* $\lim_{i\to\infty} y_i = x$. x *is therefore a boundary point of* $\overline{\mathbb{L}}_n$.

Appendix B

Assumption iii of section 2 makes $P(\cdot)$ C^∞ on T^n. Let F^{-1}: $\overline{\mathbb{L}}_n \to \mathbb{U} \subset T^n$ map the transformed space into the initial space: $F^{-1}\langle a_{n-1}, \ldots, a_{\lceil n/2 \rceil}(|a_{\lceil n/2 \rceil}|);$ $\angle a_0\rangle = \langle x^1, \ldots, x^n\rangle$ for odd (even) n, s.t, $0 \leq x^1 \leq x^2 \leq \cdots \leq x^n < 2\pi$. Boundaries of $\mathbb{U}$ are of no concern because the range of F^{-1} could equally well be $\delta \leq x^1 \leq x^2 \leq \cdots \leq x^n < 2\pi + \delta$ for arbitrary δ and $P(\cdot)$ is C^∞ on T^n. Let $G(\cdot)$ denote the Cartesian product of $F^{-1}(\cdot)$ with itself appropriately many times that maps the transformed space of all relevant neurons into their initial spaces. Define, tentatively, $\widetilde{P} = P \circ G$.

Since both P and F are C^∞, $\widetilde{P}$ is C^∞ wherever the Jacobian of F is nonsingular.

Theorem 7. $\frac{\partial x^k}{\partial a_j}$ *is undefined when* x^k *is a multiple root, that is,* $\exists a, b$ *s.t* $x^a = x^b \Rightarrow Det(DF) = 0$.

Proof. $\forall j\ a_j$ is a symmetric function of $\langle x^1, \ldots, x^n\rangle$. Therefore, $\forall j\ \frac{\partial a_j}{\partial x^a} = \frac{\partial a_j}{\partial x^b}$ when $x^a = x^b$. In other words, if $x^a = x^b$, columns a and b in (DF) are identical.

Theorem 8. $\forall i, j\ (i \neq j \Rightarrow x^i \neq x^j) \Rightarrow Det(DF) \neq 0$.

Proof. We prove the theorem for cases, n is odd and n is even, separately.

i. n is odd. Based on the functions defining coefficients in terms of roots and simple matrix manipulations, (DF) evaluated at $\langle x^1, x^2, \ldots, x^n\rangle = \langle\theta_1, \theta_2, \ldots, \theta_n\rangle$ can be reduced to the matrix $[a_{i,j}]_{1\leq i,j\leq n}$ defined as: for all $j = 1, \ldots, n$, (a) if $i = 1$, $a_{i,j} = 1$, (b) if $i > 1$ is even, $a_{i,j} = \sin(\frac{i}{2}\theta_j)$, and (c) if $i > 1$ is odd, $a_{i,j} = \cos(\frac{i-1}{2}\theta_j)$.

We prove $Det(DF) \neq 0$ by demonstrating that for any vector $\vec{x}$, $\vec{x} * [a_{i,j}]_{1\leq i,j\leq n} = 0$ implies $\vec{x} \equiv \langle 0, \ldots, 0\rangle$. Let $n = 2m + 1$, and $f(x) = \alpha_0 + \sum_{i=1}^{m} \alpha_{2i-1} \sin ix + \alpha_{2i} \cos ix$. For arbitrary reals $\alpha_0, \alpha_1, \ldots, \alpha_{2m}$ not all zero, we demonstrate that the *maximum* number of roots that $f(x)$ can have in $[0, 2\pi)$ is $2m$, thus proving the claim.

Let $g(x) = \gamma_0 + \sum_{i=1}^{m} \gamma_i \sin(ix + \beta_i)$ such that $g(x) \equiv f(x)$. Since $g(x)$ is periodic with period 2π, if $g(x)$ has μ roots in $[0, 2\pi)$ then $g^1(x) = g'(x)$ has *at least* μ roots in $[0, 2\pi)$, and since $g^1(x)$ is also periodic with period 2π, $g^2(x) = g''(x)$ has *at least* μ roots in $[0, 2\pi)$ and so on.

$g^{4k}(x) = \sum_{i=1}^{m} i^{4k}\gamma_i \sin(ix + \beta_i)$ for $k = 1, 2, \ldots$. As k rises, (a) the coefficients of $\sin(ix + \beta_i)$ for $i = 1, \ldots, (m-1)$ become negligible as compared to the coefficient of $\sin(mx + \beta_m)$, and (b) the magnitude of the gradients of $i^{4k}\gamma_i \sin(ix + \beta_i)$ for $i = 1, \ldots, (m-1)$ also become negligible as compared to the gradient of $m^{4k}\gamma_m \sin(mx + \beta_m)$ near its roots. Since $m^{4k}\gamma_m \sin(mx + \beta_m)$ has 2m roots in $[0, 2\pi)$, we have $\mu \leq 2m$.

ii. n is even. Let $n = 2m$. For any θ^*, the mapping $F\langle x^1, \ldots, x^{2m}\rangle = \langle a_{n-1}, \ldots, |a_{\lceil n/2 \rceil}|; \angle a_0\rangle$ is a C^∞-diffeomorphism in an open set about $\langle \theta_1, \theta_2, \ldots, \theta_{2m}\rangle$ if and only if the mapping $F'\langle x^1, \ldots, x^{2m}; x^{2m+1}\rangle = \langle a_{n-1}, \ldots, |a_{\lceil n/2 \rceil}|; \angle a_0; x^{2m+1}\rangle$ is a C^∞-diffeomorphism in an open set about $\langle \theta_1, \theta_2, \ldots, \theta_{2m}, \theta^*\rangle$. Consequently, all that needs to be shown is that for $n = 2m$, the mapping $\langle a_{2m-1}, \ldots, |a_m|; \angle a_0; x^{2m+1}\rangle \rightarrow \langle A_{2m}, \ldots, A_{m+1}; \angle A_0\rangle$ is C^∞ (A_i's are the coefficients of the polynomial of degree 2m+1 whose roots include the additional $e^{i\theta^*}$). Note that $\forall i, j\ (i \neq j \Rightarrow \theta_i \neq \theta_j)$ and $\forall i = 1, \ldots, 2m\ \theta_i \neq \theta^*$ is enforced by i above on the mapping $\langle A_{2m}, \ldots, A_{m+1}; \angle A_0\rangle \rightarrow \langle x^1, \ldots, x^{2m}; x^{2m+1}\rangle$.

The trivial relations between the A_i's and the a_i's immediately prove that the mapping is C^∞.

The portion of $\overline{\mathbb{L}}_n$ actually explored by the state dynamics of the neuron has multiple roots only at $e^{ix^i} = e^{ix^j} = 1$, that is, when the spikes are dead. We therefore define $\widetilde{P}(\cdot)$ as follows:

1. If $\forall$ relevant i each $\langle x_i^1, x_i^2, \ldots, x_i^{n_i}\rangle$ is composed of distinct elements, then $\widetilde{P}(\cdot)$ is C^∞ as demonstrated in the preceding theorem.
2. If $\exists$ relevant i s.t $\langle x_i^1, x_i^2, \ldots, x_i^{n_i}\rangle$ is not composed of distinct elements, and x^* is one such multiple element (at $e^{ix^*} = 1$), then we define, for all $m, j_1, \ldots, j_{l-1}, k_1, \ldots, k_l$ (such that $\sum_{i=1}^{l} k_i = m$), and i_p^q's (not necessarily distinct, for $q = 1, \ldots, l$, $p = 1, \ldots, k_q$)

$$\frac{\partial^m P}{\partial^{k_1} x^{j_1} \ldots \partial^{k_{l-1}} x^{j_{l-1}} \partial^{k_l} x^*} \times \frac{\partial^{k_1} x^{j_1}}{\partial a_{i_1^1} \ldots \partial a_{i_{k_1}^1}} \cdots \frac{\partial^{k_{l-1}} x^{j_{l-1}}}{\partial a_{i_1^{l-1}} \ldots \partial a_{i_{k_{l-1}}^{l-1}}} \times \frac{\partial^{k_l} x^*}{\partial a_{i_1^l} \ldots \partial a_{i_{k_l}^l}} = 0. \tag{B.1}$$

Although $\frac{\partial^{k_l} x^*}{\partial a_{i_1^l} \ldots \partial a_{i_{k_l}^l}}$ is undefined in such a case, by imposing the additional constraint $\frac{\partial P}{\partial x^*} = 0$ over an infinitesimal interval ($e^{i\delta} > e^{ix^*} > e^{i(2\pi - \delta)}$) irrespective of the values assigned to the other variables,

we can maintain infinite differentiability of $\widetilde{P}$, since we then have $\frac{\partial^m P}{\partial^{k_1} x^{j_1} \ldots \partial^{k_{l-1}} x^{j_{l-1}} \partial^{k_l} x^*} = 0$ over the interval.

3. If $\exists$ relevant i s.t $\langle x_i^1, x_i^2, \ldots, x_i^{n_i} \rangle$ is not composed of distinct elements, but member element x^* is a distinct element, then $\frac{\partial x^*}{\partial a_j}$ cannot be directly computed from $(DF)^{-1}$ since $det(DF) = 0$. However, as is shown next, tangible value exists for $\frac{\partial x^*}{\partial a_j}$. It is also shown that $\frac{\partial x^*}{\partial a_j}$ is C^∞.

Theorem 9. *Let the roots of* $f(z) = z^n + a_{n-1}z^{n-1} + \cdots + a_0$, *constrained to lie on* $|z| = 1$, *be* $\langle e^{ix^1}, e^{ix^2}, \ldots, e^{ix^n} \rangle$. *Let* $e^{ix^a} = e^{ix^b}$ *and all other roots be distinct. Let the sequence of sets* $\langle y_p^1, y_p^2, \ldots, y_p^n \rangle$ *for* $p = 1, 2, \ldots$ *be constructed s.t* $\forall p, q\ y_p^q$ *is distinct,* $\forall q\ \lim_{p\to\infty} y_p^q = x^q$. *Then* $\forall p\ (DF)^{-1}|_{\langle y_p^1, y_p^2, \ldots, y_p^n \rangle}$ *is well defined and limiting values exist for* $\frac{\partial x^k}{\partial a_j}$ *for all* $k \neq a$ *or b. Moreover,* $\frac{\partial x^k}{\partial a_j}$ *is* C^∞ *for all such values of k.*

Proof. That $\forall p\ (DF)^{-1}|_{\langle y_p^1, y_p^2, \ldots, y_p^n \rangle}$ is well defined follows from the previous theorem. Just as in the previous theorem, we consider the case for odd n first. We refer to the simplified version of (DF) evaluated at $\langle \theta_1, \theta_2, \ldots, \theta_n \rangle$ given earlier. In the limit, column b can be replaced by ($\frac{d}{d\theta}$ column a) $\equiv \langle 0, \cos(\theta_a), -\sin(\theta_a), 2\cos(2\theta_a), -2\sin(2\theta_a), \ldots \rangle^T$.

We demonstrate that this matrix is invertible. Let $g(x) = \gamma_0 + \sum_{i=1}^m \gamma_i \sin(ix + \beta_i)$. For arbitrary reals $\gamma_0, \gamma_1, \beta_1, \ldots, \gamma_m, \beta_m$ not all zero, $g(x)$ cannot have $2m$ distinct roots and one multiple root in $[0, 2\pi)$ because $g^1(x)$ must then have at least $2m + 1$ roots in $[0, 2\pi)$ and so on.

All rows except a and b in $(DF)^{-1}$, computed as $(DF)^{-1}(DF) = I$, therefore have finite limiting values, identical to the corresponding values in the inverse of the matrix described above. Since the elements of the matrix are C^∞, and its determinant (a C^∞ function of its elements) is nonzero, the elements of its inverse are C^∞.

The case for even n is treated exactly as in the previous theorem.

References

Aertsen, A., & Braitenberg, V. (1992). *Information processing in the cortex: Experiments and theory.* Berlin: Springer-Verlag.

Amit, D. J., Gutfreund, H., & Sompolinsky, H. (1987). Information storage in neural networks with low levels of activity. *Phys. Rev. A, 35*(5), 2293–2303.

Babloyantz, A., Salazar, J. M., & Nicolis, C. (1985). Evidence of chaotic dynamics of brain activity during the sleep cycle. *Phys. Lett. A, 111*, 152–156.

Bair, W., & Koch, C. (1996). Temporal precision of spike trains in extrastriate cortex of the behaving macaque monkey. *Neural Comp., 8*, 1185–1202.

Bair, W., Koch, C., Newsome, W., & Britten, K. (1994). Reliable temporal modulation in cortical spike trains in the awake monkey. In *Proceedings of the Symposium on Dynamics of Neural Processing*.

Basar, E. (1990). *Chaos in brain function*. Berlin: Springer-Verlag,.

Bernander, O., Douglas, R. J., & Koch, C. (1992). *A model of regular-firing cortical pyramidal neurons* (CNS Memo 16). Pasadena: California Institute of Technology.

Bower, J. M., & Beeman, D. (1995). *The book of GENESIS: Exploring realistic neural models with the GEneral NEural SImulation System*. New York: TELOS/Springer-Verlag.

Braitenberg, V. (1978). Cortical architectonics: General and area. In M. A. B. Brazier & H. Petsche (Eds.), *Architectonics of the cerebral cortex* (pp. 443–465). New York: Raven Press.

Braitenberg, V., & Schüz, A. (1991). *Anatomy of the cortex: Statistics and geometry*. Berlin: Springer-Verlag.

Burns, B., & Webb, A. C. (1976). The spontaneous activity of neurones in the cat's cerebral cortex. *Proc. Royal Soc. London (Biol.), 194*, 211–223.

Cohn, A. (1922). Uber die anzahl der wurzeln einer algebraischen gleichung in einem kreise. *Math. Zeit*, *14*, 110–148.

Coolidge, J. L. (1908). The continuity of the roots of an algebraic equation. *Annals of Math. (series 2)*, *9*, 116–118.

Erdi, P. (1996). Levels, models, and brain activities: Neurodynamics is pluralistic (open peer commentary). *Behav. and Brain Sci.*, *19*, 296–297.

Freeman, W. J. (1991). Predictions on neocortical dynamics derived from studies in paleocortex. In E. Basar and T. H. Bullock (Eds.), *Induced rhythms of the brain* (pp. 183–199). Cambridge, MA: Birkhauser Boston.

Hines, M. (1993). NEURON—A program for simulation of nerve equations. In F. Eckman (Ed.), *Neural systems: Analysis and modeling* (pp. 127–136). Norwell, MA: Kluwer.

Hopfield, J. (1982). Neural networks and physical systems with emergent collective computational abilities. *Proc. Natl. Acad. Sci. U.S.A., 79*, 2554–2558.

Hornik, K., Stinhcombe, M., & White, H. (1989). Multilayer feedforward networks are universal approximators. *Neural Networks, 2*, 359–366.

Krüger, J. (1991a). *Neuronal cooperativity*. Berlin: Springer-Verlag.

Krüger, J. (1991b). Spike train correlation on slow time scales in monkey visual cortex. In J. Krüger (Ed.), *Neuronal cooperativity*. Berlin: Springer-Verlag.

MacGregor, R. J., & Lewis, E. R. (1977). *Neural modeling*. New York: Plenum Press.

Marden, M. (1948). The number of zeros of a polynomial in a circle. *Proc. Natl. Acad. Sci. U.S.A.*, *34*, 15–17.

Nunez, P. L. (1989). Generation of human EEG by a combination of long and short range neocortical interactions. *Brain Topography, 1*, 199–215.

Omlin, C. W., & Giles, C. L. (1996). Constructing deterministic finite-state automata in recurrent neural networks. *J. ACM*, *43*, 937–972.

Peters, A., & Proskauer, C. C. (1980). Synaptic relationships between a multipolar stellate cell and a pyramidal neuron in the rat visual cortex: A combined golgi-electron microscope study. *J. Neurocytol., 9*, 163–183.

Peters, A., & Regidor, J. (1981). A reassessment of the forms of nonpyramidal neurons in area 17 of cat visual cortex. *J. Comp. Neurol., 203*, 685–716.

Röschke, J., & Basar, E. (1989). Correlation dimensions in various parts of cat and human brain in different states. In E. Basar and T. H. Bullock (Eds.), *Brain dynamics* (pp. 131–148). Berlin: Springer-Verlag.

Schüz, A. (1992). Randomness and constraints in the cortical neuropil. In A. Aertsen and V. Braitenberg (Eds.), *Information processing in the cortex* (pp. 3–21). Berlin: Springer-Verlag.

Shepherd, G. M. (1998). *The synaptic organization of the brain*. New York: Oxford University Press.

Siegelmann, H. T., & Sontag, E. D. (1992). On the computational power of neural-nets. In *Proceedings of the Fifth ACM Workshop on Computational Learning Theory* (Pittsburgh, PA).

Softky, W. R., & Koch, C. (1993). The highly irregular firing of cortical-cells is inconsistent with temporal integration of random EPSPs. *J. Neurosci., 13*, 334–350.

Strehler, B. L., & Lestienne, R. (1986). Evidence on precise time-coded symbols and memory of patterns in monkey cortical neuronal spike trains. *Proc. Natl. Acad. Sci. U.S.A., 83*, 9812–9816.

Wright, J. J. (1990). Reticular activation and the dynamics of neuronal networks. *Biol. Cybern., 62*, 289–298.

Received June 14, 1999; accepted May 1, 2000.